AALBORG UNIVERSITY
STUDENT REPORT

Diffuse ceiling ventilation - Experimental and numerical analysis based on variation of room geometry and heat load distribution

Rasmus Westh Vilsbøll

Master's Thesis

Indoor Environmental and Energy Engineering

Department of Civil Engineering

Aalborg University

Completed 6th of June, 2014

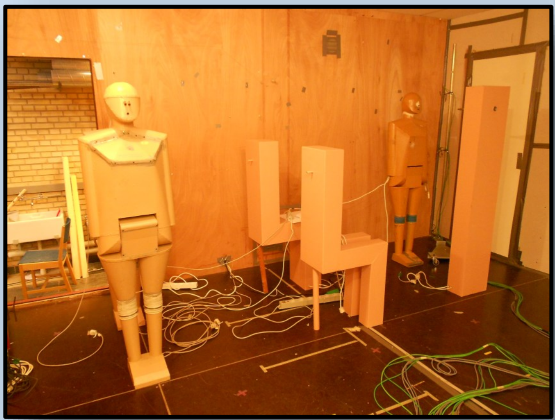

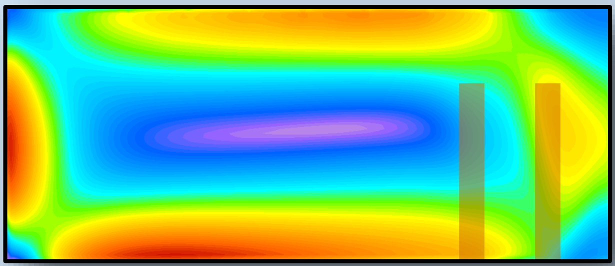

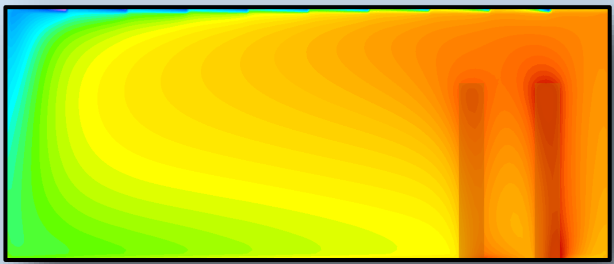

Aalborg University
School of Engineering and Science
Sohngårdsholmsvej 57
9000 Aalborg
Phone No.: +45 99 40 85 30
http://www.ses.aau.dk

AALBORG UNIVERSITY
STUDENT REPORT

Title:
Diffuse ceiling ventilation - Experimental and numerical analysis based on variation of room geometry and heat load distribution

Project period:
September 2013 - June 2014

Project group:
B-223b

Author:

Rasmus Westh Vilsbøll

Supervisors:
Peter Vilhelm Nielsen
Li Liu

Editions: 4

Number of pages: 76

Number of appendix pages: 22

Appendix CD

Completed: 6th of June 2014

Synopsis:

This report contains an analysis of the performance of diffuse ceiling ventilation in a room with varying heat load distribution, room height and air supply geometry. First it is tested whether or not the similarity principle is applicable, followed by detailed comparisons mainly based on cooling capacity but also air velocity and temperature distribution. Three different heat load distributions and three different room heights with varying ceiling geometry are tested. To support the experimental results, numerical analysis is conducted by means of CFD simulations.

The content of this report is freely available, but publication with the source references should only be done in agreement with the author.

Abstract

A continuously growing focus on lowering the energy consumption and improving the indoor climate gives challenges when designing buildings. In densely occupied spaces, large amounts of fresh air must be supplied to keep a good indoor air quality, often with the result that draught or high temperature gradients occur. Diffuse ceiling ventilation is an air distribution system in which the air is supplied from the entire ceiling surface, giving a low supply velocity. Therefore the flow pattern in the room is controlled by the present heat sources. The system typically generates high mixing and the air velocities in the room are expected not to be influenced by the flow rate to the room. Previous studies have shown that diffuse ceiling ventilation has an ability to remove large heat loads without compromising the indoor climate, however recent experiments indicate that problems can occur at large room height and with certain heat load distributions.

The experimental part in this thesis is an investigation of the importance of three parameters: room height, heat load distribution and air supply geometry. Results consist of measured air velocities and temperatures in the test room and are evaluated using a method where the thermal climate in the room determines the cooling capacity of the system. The results of the measurements showed that both room height and heat load distribution had great importance on the performance of the system, but also that air velocities in the room increased when increasing the flow rate opposite previous experimental investigations.

CFD simulations were set up in the program FloVENT to either further investigate the nature of the flow in some experimental situations. A reference model with conditions similar to one of the experiments was created, and validation showed good accordance between experiments and CFD model. The reference model was modified to test some tendencies experienced in the experiments, namely what happens when changing flow rate, room height or supply geometry. The CFD predictions showed very similar results as the experiments. Air velocities in the room was dependent on the flow rate, and room height had a great significance on the thermal indoor climate in the room. It also showed very vague changes when changing supply geometry from small slot diffusers to a fully diffuse ceiling.

Abstract in Danish

Større fokus på reducering af energiforbruget og forbedring af indeklimaet giver udfordringer i bygningers designfase. I rum med store personbelastninger skal store ventilationsmængder til, for at opretholde en god luftkvalitet, ofte med det resultat at træk eller høje temperaturgradienter opstår. Diffus loftindblæsning er et ventilationssystem, hvor frisk luft blæses ind gennem loftet, hvilket giver en lav indblæsningshastighed, selv ved høje luftmængder. Luftstrømningerne i rummet er derfor kontrolleret af den termiske belastning. Typisk genererer systemet god opblanding og de lufthastigheder, der opleves i opholdszonen påvirkes ikke af hvor stor luftmængde, der tilføres rummet. Tidligere undersøgelser har vist, at diffus loftindblæsning har evnen til at fjerne store termiske belastninger uden at forringe indeklimaet. Nyere forsøg har dog indikeret, at problemer kan opstå ved store rumhøjder og ved visse fordelinger af varmebelastninger.

Den eksperimentelle del af denne afhandling er en undersøgelse af vigtigheden af tre parametre: rumhøjde, fordeling af varmebelastninger og indblæsningsgeometri. Resultaterne består af målte lufthastigheder og temperaturer i testrummet og er evalueret vha. en metode hvor det termiske indeklima angiver systemets køleevne. Resultaterne viste at både rumhøjde og placering af varmebelastninger havde en stor påvirkning påsystemets evne til at fjerne varmebelastninger uden at skabe træk, men også at lufthastighederne steg, når luftmængden til rummet blev større, modsat tidligere undersøgelser.

CFD simuleringer er foretaget i programmet FloVENT for at uddybe forståelsen for luftstrømningerne i nogle af eksperimenterne. En referencemodel med ens randbetingelser som et af forsøgene blev lavet, og validering med de eksperimentelle resultater viste god sammenhæng. Referencemodellen var herefter modificeret for at teste nogle af de tendenser, der blev oplevet under målingerne. Modellerne skulle hjælpe til at forstå, hvad der skete ved ændring af luftmængde, rumhøjde eller indblæsningsgeometri. CFD simuleringerne viste god sammenhæng mellem målinger og numeriske modeller. Lufthastighederne i rummet var afhængige af luftmængden, og rumhøjde havde en stor betydning på indeklimaet. Ændring af indblæsningsgeometri havde ikke nogen særlig virkning i det omfang den blev ændret.

Preface

This report is a Master's Thesis. It is a documentation of the work carried out in the project "Diffuse ceiling ventilation - Experimental and numerical analysis based on variation of room geometry and heat load distribution" from September 2013 to June 2014. The project was written in the Master of Science programme at the faculty of Indoor Environmental and Energy Engineering at the Department of Civil Engineering at Aalborg University.
The project originated in several earlier studies regarding diffuse ceiling ventilation. The work in this thesis was to investigate the importance of different parameters influencing the performance of diffuse ceiling ventilation, namely positions of heat sources, room height and supply geometry.
The report consists of experimental studies conducted in a laboratory supported by numerical analysis by means of CFD simulations. After the main report an appendix report follows, giving further insight in experiments and CFD simulations.

I would like to thank my supervisors - Professor Peter Vilhelm Nielsen and Assistant Professor Li Liu, whose knowledge and experience it has been a privilege to have access to, and for the time they have spent giving much appreciated guidance.

Reading guide

The report is divided into two main parts - a main report and an appendix report. The main report contains the theoretical background, experimental set-up and results and CFD predictions. The appendix report contains supplementary drawings, theory and equipment descriptions.
Furthermore an Appendix CD is attached to the back of the report. It contains calculations, CFD models, drawings and other relevant information that is not included in the report or appendix. References to the Appendix CD are made throughout the report and the table of content for the Appendix CD is located in Appendix A.

Chapters are numbered chronologically and their figures, tables and equations are numbered according to the number of the chapter in which they appear. Thus, the first figure in Chapter 2 will be named figure 2.1, the second figure 2.2 and so on. Explanations of figures and tables are located below each individual figure, where also references to rightful owners are located in case the material is not created by the author.

The reference will be referred to as [Surname, Year] for books, norms and instructions as [Title, Year] and websites as [Website name, Year]. If references appear directly in a context, the brackets will only appear for the production year, meaning a book will be referred to as Surname, [Year]. The sources are completely listed in the bibliography in the end of the report, where books are listed with the name of the author, title, edition, publication date and publisher. Web pages are listed with author, title, year and date of visit. Any content made exclusively by the author will not contain any reference.

Symbols and units

Symbols

A	Area	[m^2]
Ar	Archimedes number	[-]
β	Expansion coefficient	[1/K]
c_p	Specific heat capacity	[J/kg K]
ϵ	Dissipation rate of turbulent kinetic energy	[W/kg]
Φ	Power	[W]
g	Gravitational acceleration	[m/s^2]
h	Height	[m]
H	Height	[m]
k	Turbulent kinetic energy	[J/kg]
l	Reference length	[m]
l_l	Turbulent length scale	[m]
M	Activity level	[met]
n	Quantity of variable	[-]
ν	Kinematic viscosity	[m^2/s]
p	Pressure	[Pa]
q	Volumetric flow rate	[m^3/s]
Re	Reynolds number	[-]
ρ	Density	[kg/m^3]
STD	Standard deviation	[m/s]
T	Temperature	[K]
t	Temperature	[°C]
Tu	Turbulence intensity	[%]
u	Air velocity	[m/s]
$\overline{u}$	Mean air velocity	[m/s]

Sub- and superscripts

$*$	Dimensionless
l	Local
0	Supply
s	Supply
e	Extract
OCZ	Occupied zone
lab	Laboratory
rm	Occupied zone maximum

Acronyms

ACH	Air Change Rate
CFD	Computational Fluid Dynamics
CV	Control Volume
DCV	Diffuse Ceiling Ventilation
DR	Draught Rate
FVM	Finite Volume Method
IAQ	Indoor Air Quality
OCZ	Occupied Zone
PMV	Predicted Mean Vote
PPD	Predicted Percentage of Dissatisfied
RTA	Radiant Temperature Asymmetry
VTG	Vertical Temperature Gradient

Contents

F CFD in FloVENT

G CFD - Grid independence

Introduction 1

This chapter contains an introduction to diffuse ceiling ventilation and what advantages and disadvantages can follow the use of diffuse ceiling ventilation. Furthermore a problem definition will describe the scope of the investigations which will be conducted.

1.1 Introduction

For every year passing, the demands for tightness of buildings increase with the main objective of lowering the use of energy for heating. To meet those demands, buildings have to be ventilated at a greater rate and for longer periods over the year. The need for mechanical ventilation will only grow in the future making the choice of the most suitable ventilation system pivotal for obtaining the wanted indoor climate and at the same time keeping the energy consumption low. Simultaneously, demands for both thermal and atmospheric indoor climate increase for which reason the ventilation system not only needs to remove excess heat and atmospheric emissions, but also to ensure that draught and high temperature differences do not occur in occupied spaces. A way to accommodate these demands may be to raise the efficacy of the ventilation system.

When talking about comfort ventilation in general, traditional displacement ventilation is known for having a very high ventilation effectiveness which means it's ability to remove heat and atmospheric emissions is high. However this advantage does bring some downsides, for instance large temperature differences. This also applies with mixing ventilation, though the effectiveness is lower due to the mixing of air in the room. A typical problem is that air supplied with relatively high velocity often causes both draught and noise issues. Using the engine of displacement ventilation - the heat sources - and low air velocities combined with the mixing principle from mixing ventilation will yield a system that creates a low amount of draught but maintains the ability of removing large heat loads. Diffuse ceiling ventilation is a type of air distribution that can meet these demands.

1.2 Problem definition

Diffuse ceiling ventilation (DCV) is an air distribution system in which the air is supplied through the ceiling. Different applications of DCV is investigated in this master's thesis. In Denmark, DCV is commonly used in livestock buildings, but it's potential in comfort ventilation seems underrated and it is believed that DCV has a much higher potential than presumed by many. The ability of the system to remove heat is very useful in rooms with high person and equipment loads, i.e. offices, classrooms, lecture rooms, museums and others. DCV is expected to become more widely used in the future, also when considering the increasing demands for indoor climate.

In recent years several full-scale investigations of diffuse ceiling have been conducted, generally with the conclusion that the system excels in removing heat without impairing the thermal comfort of occupants. Although DCV is believed to be a solution of both present and future, it has in some situations shown a significant decrease in performance, resulting in draught in the room even at low thermal loads. Hopefully the investigations conducted in this thesis will widen the knowledge about diffuse ceiling ventilation and reveal situations in which the system does not perform as expected.

The main investigations regard testing which of the following three factors influence the indoor climate the most - and to what extend:

- Room height
- Heat load distribution
- Supply geometry

Investigations are conducted mainly through experimental studies in a test chamber with diffuse ceiling ventilation and, to support the experiments, numerical studies by means of CFD simulations.

Review of previous studies 2

In recent years several studies concerning diffuse ceiling ventilation have been conducted. In this chapter, a design chart used for comparing different types of air distribution systems is described and subsequently, a short survey of the most essential conclusions of the past studies with diffuse ceiling are presented.

2.1 Analysis and design of room air distribution systems

Observing a given room, depending on the type of air distribution system used, air is supplied differently into the occupied space. Popular and traditional types of mechanical comfort ventilation systems are mixing or displacement ventilation. The main tasks for these systems are to supply fresh air and remove heat, gases, and particles which are emitted in the building. However, just supplying fresh air into a room is not sufficient - another necessity is that the occupants should experience high air quality and thermal comfort in the occupied zone. The way the air is supplied into the room has great significance regarding the comfort of the occupants. Since each type of air distribution system has it's advantages and disadvantages, in a design phase it is important to consider which type suits the case in hand best. Other than indoor climate, also the energy consumption of the system needs to be considered. Many indoor climate factors can be considered in a design phase of air distribution systems and relevant ones are described in chapter 3.

2.1.1 The occupied zone

The occupied zone is an imaginary volume of a given room in which the occupants are expected to reside during the time they stay in the room. The reasons for using a bound volume are that the occupants of a room typically stay within the boundaries of the occupied zone and because the conditions outside the zone, for instance close to windows, walls or ceiling can be difficult to keep at an acceptable comfort level. The occupied zone can be regarded as a volume in which the requirements of the indoor climate must be fulfilled. Therefore, only a part of the room needs to be taken into consideration when evaluating the conditions in a room.

DS/EN 13779 [2007] states that "*the occupied zone in a room is that space in which the occupants are normally located and where the requirements for the indoor environment shall be satisfied.*". Default distances from the physical boundaries of a room in a non-residential building are stated in table 2.1 and an example is shown in figure 2.1 on the following page. [DS/EN 13779, 2007]

Distance from inner surface	Typical range [m]	Default value [m]
Floor (lower boundary)	0 - 0.2	0.05
Floor (upper boundary)	1.3 - 2.0	1.8
External windows and doors	0.5 - 1.5	1.0
External and internal walls	0.15 - 0.75	0.5

Table 2.1. Suggested boundaries of the occupied zone. [DS/EN 13779, 2007]

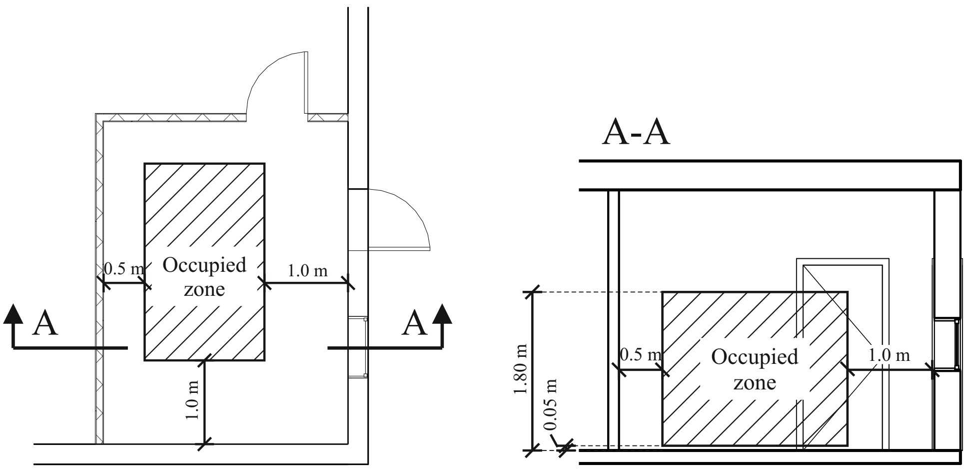

(a) Plan view of occupied zone.

(b) Sectional view of occupied zone.

Figure 2.1. Default distances defining the occupied zone in an exemplary room for non-residential building. [DS/EN 13779, 2007]

2.1.2 Flow elements

Normally air distribution systems are designed based on flow elements such as the supply air velocity from a diffuser. The borders of the occupied zone are observed, since this is where the highest velocities typically occur. This is exemplified by mixing and displacement ventilation as shown in figure 2.2 where u_{OCZ} indicates the velocity of the supplied air as it enters the occupied zone.

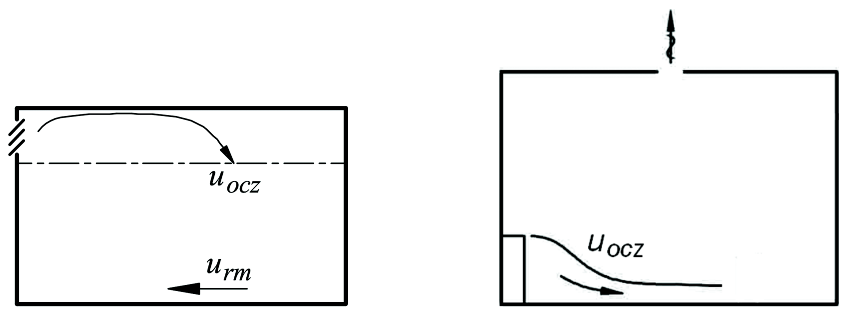

(a) Mixing ventilation.

(b) Displacement ventilation.

Figure 2.2. Possible locations of maximum velocities when considering design of mixing and displacement ventilation. u_{OCZ} indicates the velocity of supplied air when it enters the occupied zone. u_{rm} indicates the maximum velocity in the occupied zone. [Nielsen, 2007]

In the cases above, the selection of diffuser type, flow rate and temperature should be made so that the velocity u_{OCZ} at the imaginary boundary of the occupied zone has an acceptable level.In case of mixing and especially displacement ventilation, this design procedure is well accepted since u_{rm} in most cases will be equal to u_{OCZ} because the air is supplied more or less directly into the occupied zone. Often when using mixing ventilation, thermal plumes from occupants deflect the downward flow (high supply diffuser position) so the highest velocities in the occupied zone occur close to the floor. However, another type of vertical air distribution system as for instance diffuse ceiling ventilation has a very low inlet air velocity for which reason u_{rm} often occurs in other locations than on the border of the occupied zone. Therefore, u_{OCZ} is rarely a useful expression for the highest air velocity in the room. As a consequence of low momentum flow from the supply diffuser due to the large area of the ceiling surface, the air flow in the room is mainly if not totally controlled by heat sources. Therefore, another design method for diffuse ceiling ventilation has to be used. [Nielsen, 2007]

2.1.3 Design chart

When designing an air distribution system, it is important to find the limits of the system while maintaining an acceptable comfort level in the room. The limits refer to the flow rate that passes through the room and the temperature difference between supply and return. The system can be evaluated on basis of the thermal comfort level meaning low air velocities and low vertical temperature gradients in the room. Nielsen [2007] developed a design chart that enables for an easier selection of the air distribution system which is best suited to cover the demands for a given situation and still maintain an acceptable comfort level. The design chart can be expressed as a q_0 - ΔT_0 chart, because it graphically shows the limits of flow rate q_0 and temperature difference between supply and return ΔT_0 for any air distribution system in a given room. A q_0 - ΔT_0 chart is shown in figure 2.3.

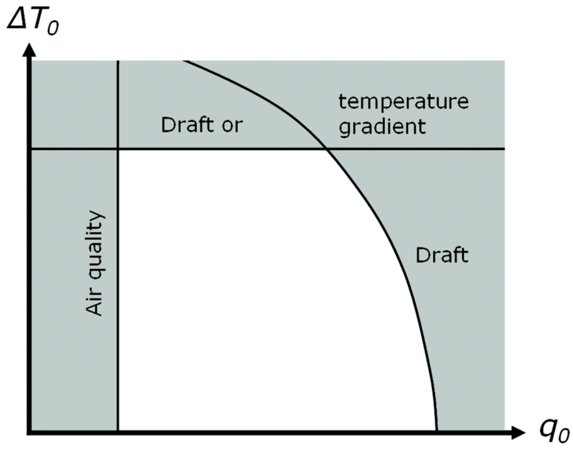

Figure 2.3. Design chart showing the limits of the flow rate q_0 and temperature difference ΔT_0 with respect to air quality, draught and temperature gradient. [Nielsen, 2007]

Figure 2.3 shows the restrictions on flow rate and temperature difference between supply and return. In other words, if flow rate or temperature difference exceeds the lower or upper limits, one can expect poor indoor air quality or draught or large temperature gradients, respectively.

Saying the graph above is general is true when considering both displacement ventilation and especially mixing ventilation. Both systems will typically create draught at high flow rate and displacement ventilation will generate high vertical temperature gradients at large temperature difference between supply and return. Diffuse ceiling ventilation will not create any momentum flow due to the large inlet area which in many cases is dispersed over the entire ceiling area. No significant air movement is created in the room and therefore there are no limits on q_0 and ΔT_0. Air movement, implied draught, is generated by the heat load in the room, and this will put a limit on the thermal load in the room, expressed as the product of q_0 and ΔT_0. The white area on figure 2.3 on the preceding page shows an area for flow rate q_0 and temperature difference between supply and return ΔT_0 in which the room is supplied with enough fresh air to obtain an acceptable air quality and simultaneously be draught-free and without large temperature gradients.
Another design graph, also taking into consideration the maximum cooling capacity is shown in figure 2.4. The maximum cooling capacity is defined as the limit at which the indoor climate becomes unacceptable due to either draught or temperature gradients. [Nielsen, 2007]

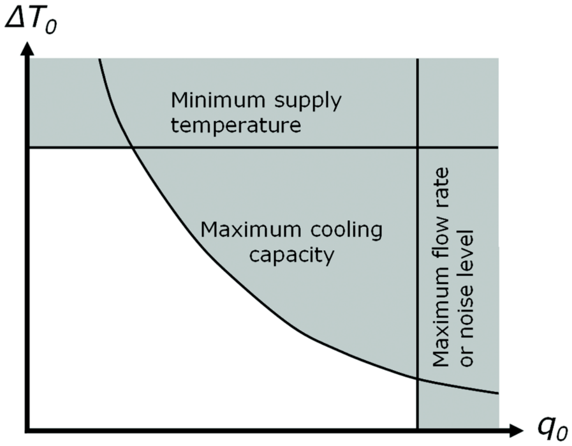

Figure 2.4. Design chart showing the limits of the flow rate q_0 and temperature difference ΔT_0 with respect to maximum cooling capacity. [Nielsen, 2007]

When supplying air into a space, the airflow pattern is controlled by either buoyancy forces or momentum forces and the ratio between these forces is called Archimedes number, Ar. The Reynolds number, Re, describes the ratio between momentum forces and viscous forces. Both numbers are dimensionless numbers and shown in equations 2.1 and 2.2. [Nielsen, 1999]

$$\mathrm{Ar} = \frac{\beta g l \Delta T_0}{u_0^2} \tag{2.1}$$

$$\mathrm{Re} = \frac{u_0 l}{\nu} \tag{2.2}$$

Where:

Ar	Archimedes number [-]
β	Expansion coefficient [1/K]
g	Gravitational acceleration [m/s^2]
l	Characteristic length, typically diffuser dimensions, h_0 or $\sqrt{a_0}$ [m]
ΔT_0	Temperature difference between supply and return flow [K]
u_0	Supply velocity [m/s]
Re	Reynolds number [-]
ν	Kinematic viscosity ($\nu = \mu/\rho$) [m^2/s]

For a given room, the expansion coefficient, gravitational acceleration and characteristic length can be considered as constants, meaning they have no significant influence on changes in the Archimedes number (changes in supply flow rate or temperature). The supply velocity is equal to the supply flow rate divided by diffuser area as shown in equation 2.3 [Nielsen, 1999].

$$u_0 = \frac{q_0}{a_0} \tag{2.3}$$

Since the other variables in Archimedes number are constants, the Archimedes number can be simplified to only be a function of the temperature difference between supply and return, and the supply flow rate, see equation 2.4 [Nielsen, 2007].

$$Ar = func\left(\frac{\Delta T_0}{q_0^2}\right) \tag{2.4}$$

When the airflow in a room is fully developed turbulent flow, the Reynolds number is high, or above a critical value. This means variables like temperature and air velocity are not dependent on the Reynolds number, however still dependent on Archimedes number. If the flow is fully developed turbulent flow, any non-dimensional velocity can be given as a function of Archimedes number if the flow is non-isothermal. This phenomenon is called the similarity principle and can be used to investigate the limits of the air distribution system with regard to supply flow and temperature difference between supply and return. [Nielsen, 2007]

A very important parameter to observe when analyzing the thermal comfort is the air velocity. Any maximum acceptable air velocity can be chosen, but for the explanation of the design procedure a velocity of 0.15 m/s is selected. The limits on flow rate and temperature difference between supply and return of the air distribution system are wanted and by limits mean that the air velocity in the room is not allowed to exceed 0.15 m/s. One can conduct an experiment at a given q_0 and ΔT_0, obtaining a maximum velocity in the occupied zone of 0.15 m/s, and thereby the limits of flow rate and temperature differences are found. However, it is practically impossible to conduct experiments this way, and an easier method is introduced. Knowing the flow rate, temperature difference and heat load in a room, the flow rate and temperature difference can be recalculated to their limits when observing the measured velocities in the occupied zone. An example of this process is shown in figure 2.5. [Nielsen, 2007]

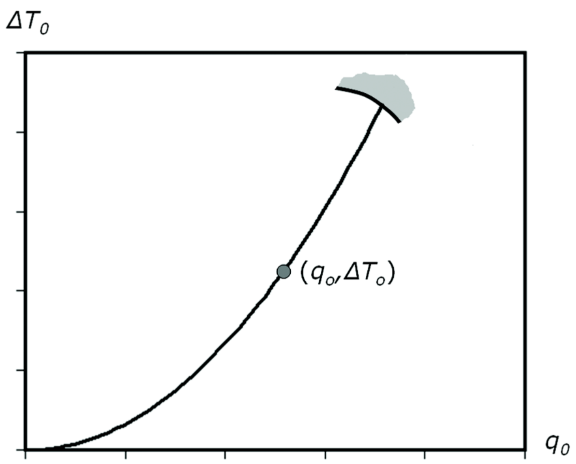

Figure 2.5. Design chart showing a given experiment (q_0,ΔT_0) and the limits on q_0 and ΔT_0. [Nielsen, 2007]

The dot on the graph in figure 2.5 is simply a given experiment (q_0,ΔT_0), the curve corresponds to a constant value of $\Delta T_0/q_0^2$, which is also a constant Archimedes number. The dimensionless equations are therefore constant along the curve, and it is possible to find the position of the limiting (q_0,ΔT_0) for a set of measurements by observing the maximum velocity in the occupied zone, although no measurements have been conducted at this particular flow rate or temperature difference.

In Nielsen [2007] five different types of air distribution systems were tested in the same room. The resulting graphs from the experiment using the above explained procedure are shown in figure 2.6 showing limits of q_0 and ΔT_0 corresponding to a maximum velocity in the occupied zone of 0.15 m/s and a maximum vertical temperature gradient of 3 K/m.

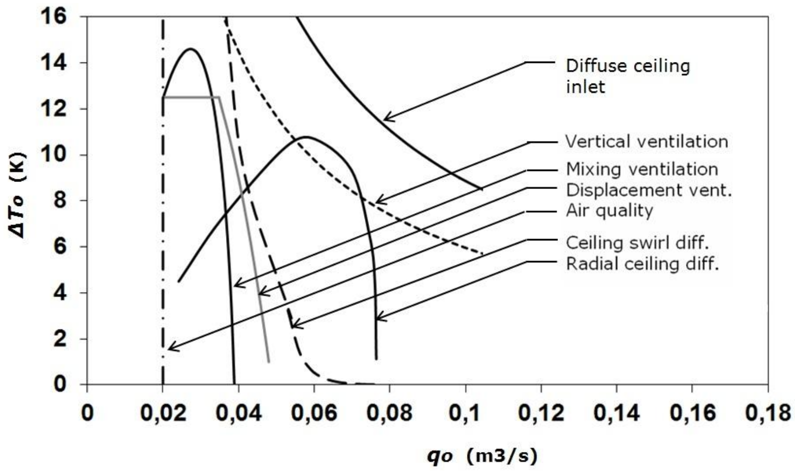

Figure 2.6. Design chart showing performance of different types of air distribution systems tested in the same room. [Nielsen, 2011]

The graphs show that diffuse ceiling inlet in the presented case could handle higher heat loads than any of the other air distribution systems.

2.2 Diffuse ceiling ventilation

Diffuse ceiling ventilation is a type of vertical ventilation where often the entire ceiling is used as the supply "opening". The air flow is controlled by either momentum flow from the air supply or buoyant flow caused by heat sources in the room. The two different variations of ceiling supplied air distribution systems are shown in figure 2.7.

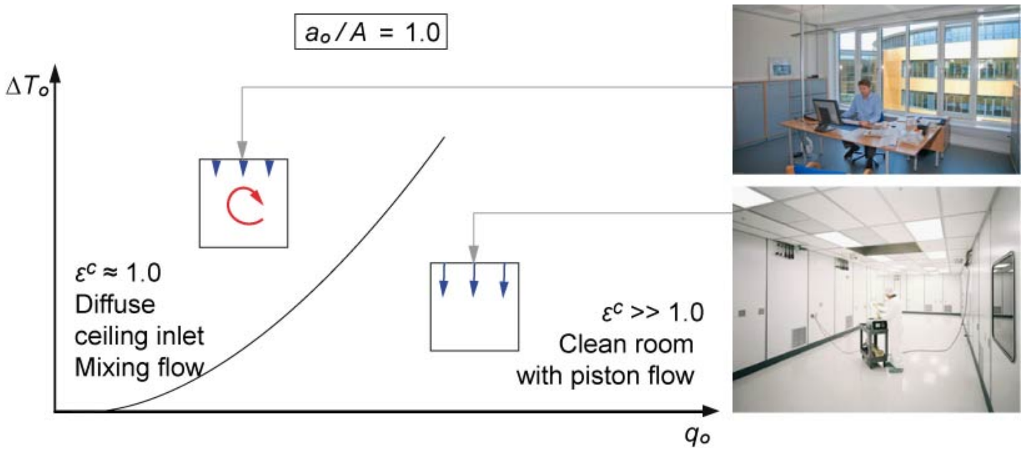

Figure 2.7. Diffuse ceiling inlet and unidirectional clean room flow, $a_0/A = 1.0$ meaning the supply area is dispersed over the entire ceiling area. The two photos show an office with diffuse ceiling inlet and a clean room with piston flow and high flow rate. [Müller et al., 2013]

On the left side of the figure the air is supplied with low momentum. Therefore, the airflow pattern is controlled by the heat loads in the room. The clean room has a much higher flow rate and the airflow is controlled by momentum rather than buoyancy. In comfort ventilation, where the momentum flow is low compared to clean room flow, high heat loads can be handled without causing draught in the occupied zone, no matter if the flow rate is high or low since the draught is created by the heat loads. The ventilation effectiveness is close to 1.0 (in cooling condition where the cold supply mixes with the thermal plumes from heat sources) with air change rates between 1 and 5 h^{-1} meaning the system performs as mixing ventilation but without the momentum flow normally characteristic for mixing ventilation. [Nielsen, 2011]

Diffuse ceiling ventilation has mainly been utilised in connection with livestock buildings but is regarded to have large potential in comfort ventilation. Several experiments have been carried out with the purpose of identifying the potential of diffuse ceiling ventilation as comfort ventilation. Some of these experiments are summarised in the following sections.

2.2.1 Offices

Both Aalborg University and the Technical University of Denmark have performed studies of diffuse ceiling ventilation in office buildings. Jakubowska [2009] conducted experiments at Aalborg University about diffuse ceiling inlet in an office with two manikins and two computers. The experimental set-up is shown in figure 2.8 on the following page.

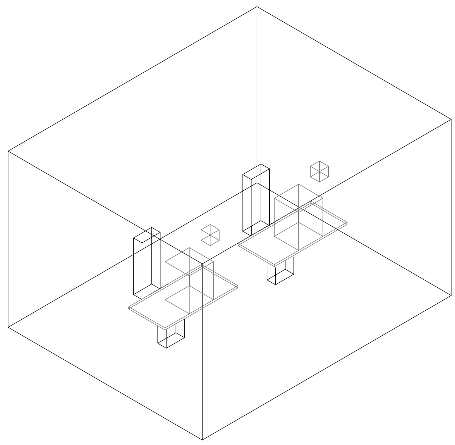

Figure 2.8. Experimental setup with two manikins, two computers and two working lamps. [Jakubowska, 2009]

The ceiling construction consisted of stone wool plates on top of small steel T-profiles. The construction of the ceiling is shown in figure 2.9.

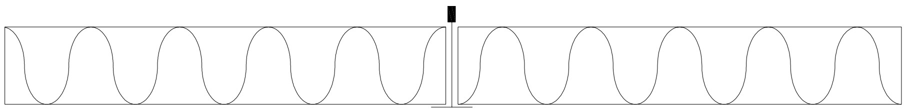

Figure 2.9. Suspended ceiling construction. Stone wool plates rest on steel T-profiles. [Jakubowska, 2009]

Experiments conducted by Jakubowska [2009] showed through smoke experiments and pressure tests that almost all air diffused through the small slots in the T-profiles between the ceiling modules rather than through the ceiling material, creating small microjets close to the ceiling. A view of the air distribution in the room is shown in figure 2.10.

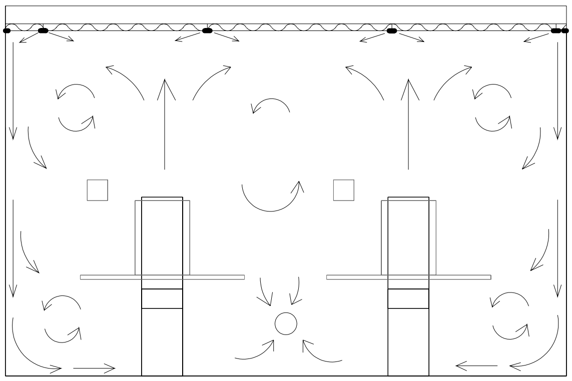

Figure 2.10. Air distribution in test room. Highest velocities occurred close to the floor. [Jakubowska, 2009]

The flow pattern in the room looks very logic - heat loads create plumes that rise in the center of the room and mixes with the colder supply air and falls down in the sides and corners of the room. Jakubowska [2009] confirmed in this study that the velocities in the room were highly dependent on the heat load in the room. This is exemplified in figure 2.11 on the next page.

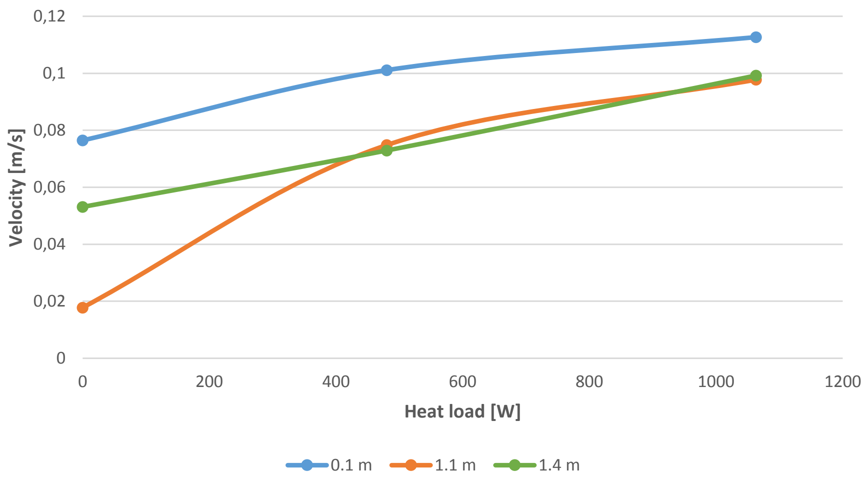

Figure 2.11. Velocities at heights of 0.1 m, 1.1 m and 1.4 m as a function of heat load. Flow rate to the room was 0.1 m^3/s. [Jakubowska, 2009]

While Jakubowska [2009] and Nielsen [2007] only investigated diffuse ceiling in the cooling condition Nielsen et al. [2010] conducted experiments in both cooling and heating situation, also at Aalborg University. The experimental setup was a little different and it is shown in figure 2.12 along with the position of measurement equipment.

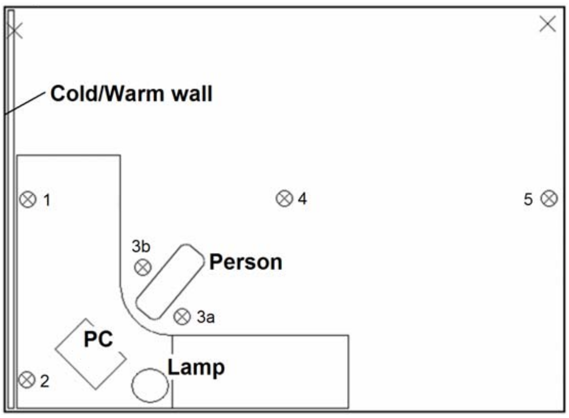

Figure 2.12. Experimental set-up. [Nielsen et al., 2010]

Smoke experiments showed that the flow in the room was controlled by the heat sources, however close to the ceiling there was a high entrainment of small microjets reaching up to 0.5 m below the ceiling. The vertical temperature gradient is shown for both cooling and heating cases. Figure 2.13 on the next page shows a cooling situation with an ACH of 8 h^{-1} and not much of a temperature gradient was present, other than in position 2, where the position of the table can have influenced the temperatures. This corresponds nicely to the fact that the room is well mixed. In this situation, heat loads were present in the room.

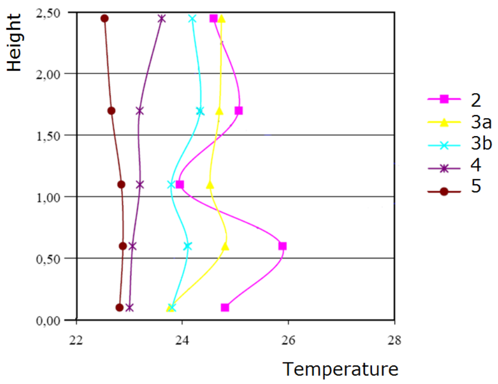

Figure 2.13. Cooling condition with an air change rate of 8.0 h^{-1}. [Nielsen et al., 2010]

A heating situation without heat loads in the room was also investigated. This was to simulate a night where the room was heated to be comfortable when people would meet in to work in the morning. The resulting temperature gradients are shown in figure 2.14 showing a larger but still acceptable vertical temperature gradient in the room. This also corresponds to one of the main assumptions behind diffuse ceiling ventilation, that heat loads control the mixing in the room, and that the air is less mixed less when they are not present. The figure also shows that changing the air change rate from 3.5 h^{-1} to 6.0 h^{-1} did not change the vertical temperature gradients in the room. The temperature gradient measured in point 1 is lower than the others because it was positioned close to a cold wall. [Nielsen et al., 2010]

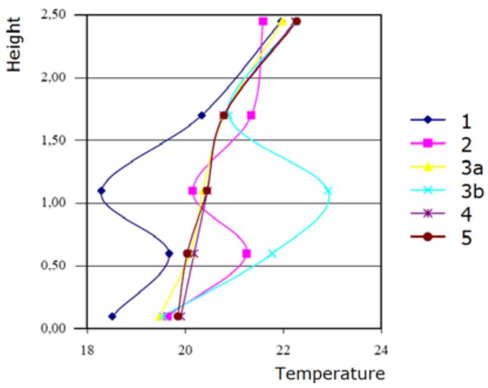

(a) Heating condition with an air change rate of 3.5 h^{-1}.

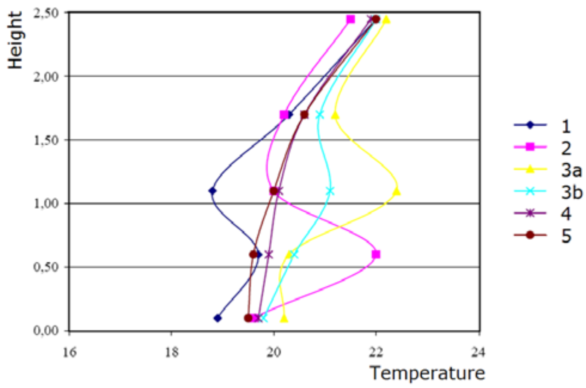

(b) Heating condition with an air change rate of 6.0 h^{-1}.

Figure 2.14. Vertical temperature gradients in heating condition. [Nielsen et al., 2010]

Finally, Yang [2011] performed experiments at the Technical University of Denmark. The experiment also included two manikins and two computers positioned symmetrically around the center of room. The main purposes of these experiments were to test the ventilation effectiveness and thermal comfort in the occupied zone. The experimental setup and ceiling construction are shown in figure 2.15 on the next page.

(a) (b)

Figure 2.15. (a) Experimental set-up and (b) ceiling construction. [Yang, 2011]

Figure 2.15(b) shows a suspended ceiling consisting of acoustic panels and below them aluminium lamellas. In the horizontal profiles carrying the acoustic panels, holes of 7 mm were drilled and below this suspended ceiling a set of aluminium lamellas were positioned. This way, the air could diffuse through the holes and down to the aluminium lamellas and leak out through the openings between the lamellas. It looks mostly like long slot diffusers stretched across the room, dispatched over the entire ceiling area. Yang [2011] measured a ventilation effectiveness very close to 1.0 at an air change rate of 3.5 h^{-1} indicating good mixing in the room. At higher air change rate the ventilation effectiveness was similar. The resulting velocities and temperature gradients in the room, shown in figure 2.16 were both within acceptable range at both low and high air change rate.

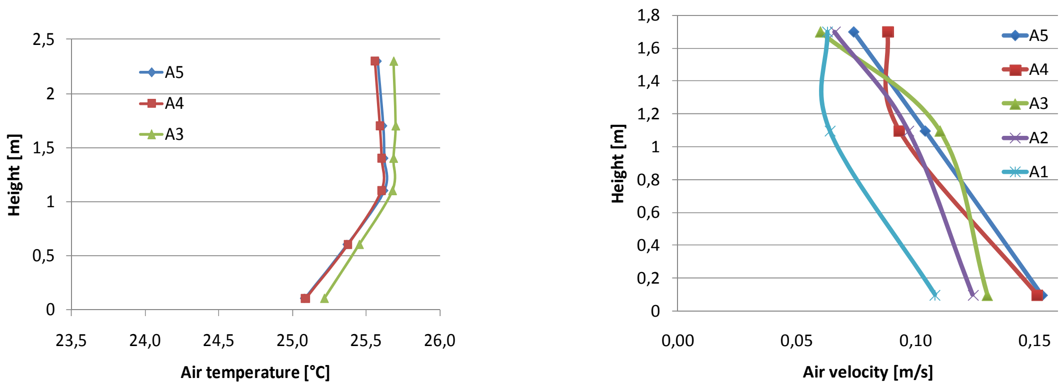

(a) (b)

Figure 2.16. (a) Vertical temperature gradient and (b) vertical velocity gradient. [Yang, 2011]

2.2.2 Schools

Due to high occupancy, classroom are very exposed to draught because in order to remove heat and CO_2, high flow rates are necessary. High flow rates are unfortunately often accompanied by high air velocities. The consequences can be high temperatures in summer and poor air quality in heating season. Jacobs et al. [2008] have investigated the potential of diffuse ceiling ventilation in classrooms in the Netherlands in a study where three different types of supply openings and two different types of heating were used. The experimental set-up and different ceiling types are shown in figure 2.17 on the following page.

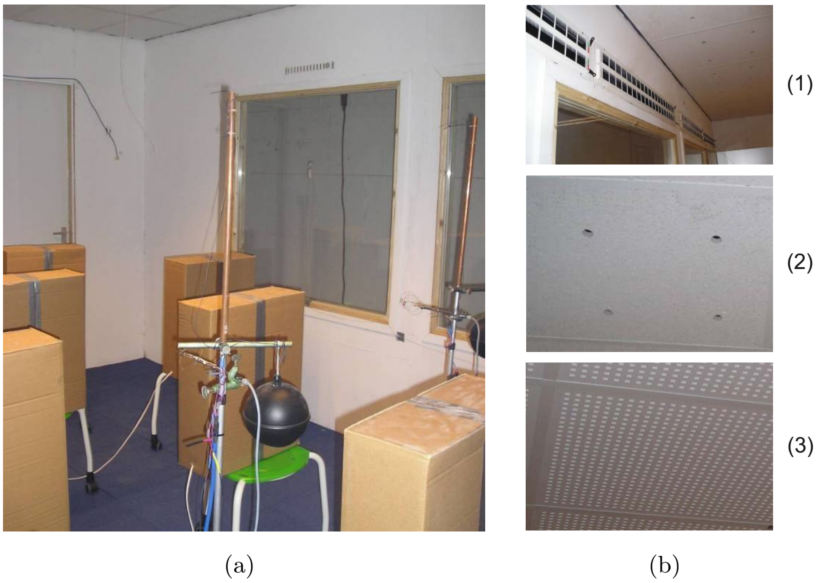

Figure 2.17. (a) Experimental setup and (b) various supply openings. (1) facade supply, (2) DCV large openings, (3) DCV small openings. [Jacobs et al., 2008]

The velocities measured in the classroom showed that the type of heating had a significant effect on the velocities, illustrated in figure 2.18.

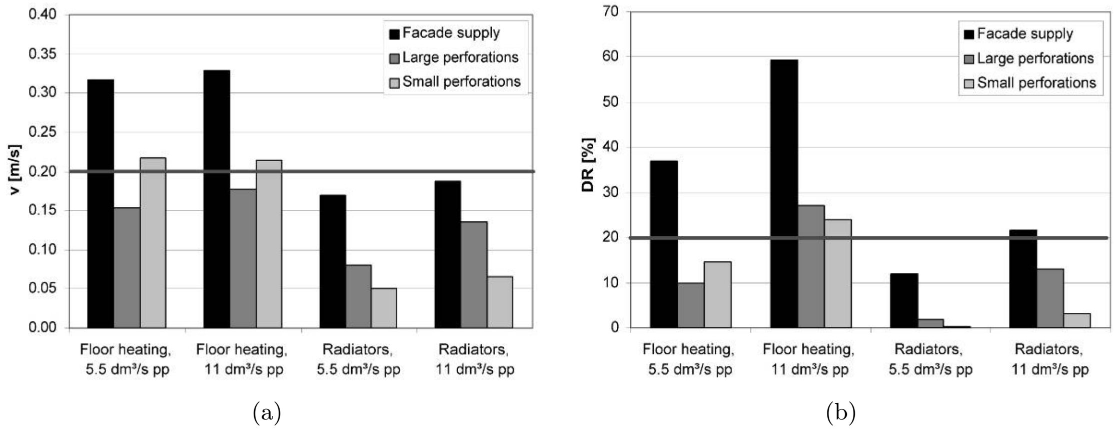

Figure 2.18. Resulting (a) velocities and (b) draught rating measured 1 m from the facade. [Jacobs et al., 2008]

The resulting velocities and draught rating shows how important positions of heat loads and supply geometry are. They also show that doubling the flow rate had no significant influence on the velocities but did affect the draught rate.

Jacobs et al. [2008] also performed full-scale experiments over six weeks in a heating period in a real classroom. The results showed that DCV successfully could be implemented in the classroom. Without creating draught the indoor air quality was improved significantly compared to a reference classroom with another, unknown type of air distribution system.

2.2.3 Museums

Also in Aalborg University, and in fact in the same facility as the undersigned have carried out experiments, Chodor and Taradajko [2013] performed similar experiments with diffuse ceiling at large room height. Investigations were carried out with the purpose of understanding the performance of diffuse ceiling inlet in a room similar to a show room in a museum. Therefore various types and positions of heat sources and varying supply area were tested. The experimental setup and different types of heat sources are shown in figure 2.19.

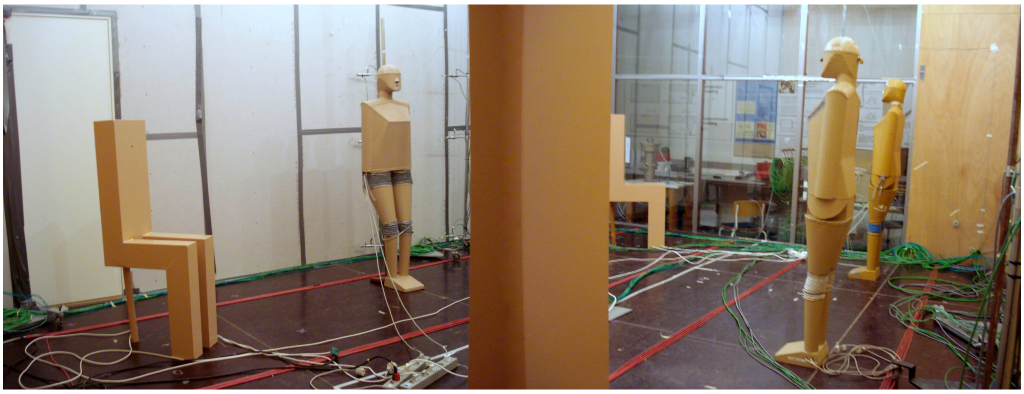

Figure 2.19. Experimental setup with manikins. Other heat sources were heating cables simulating floor heat, radiators and light bulps. [Chodor and Taradajko, 2013]

In this study the ceiling was constructed differently than in any of the previously mentioned studies. It consisted of small particles forming and a painted layer enabling air to diffuse through it. Figure 2.20 shows the construction of the ceiling and how it looked when it was installed.

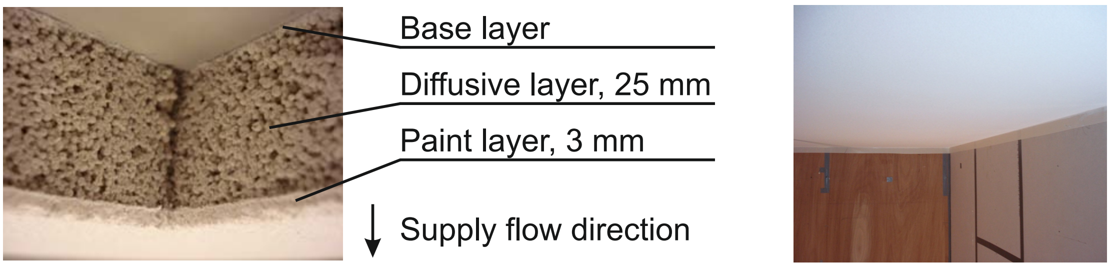

(a) Construction of diffuse ceiling. (b) Diffuse ceiling as installed.

Figure 2.20. Acoustic diffuse ceiling. The air penetrates through the small holes in the construction. [Chodor and Taradajko, 2013]

This type of ceiling looks very pleasant aesthetically, making it interesting for architects that seek a diffuser as invisible as possible. However, it also has a significantly higher pressure drop than other types of diffuse ceiling, for instance the one investigated by Jakubowska [2009], making it less energy efficient. Above the suspended ceiling, three pressure chambers were installed to make it possible to use a reduced part of the ceiling for air supply. It also enabled for testing various supply positions. The pressure chambers are shown in figure 2.21 on the following page.

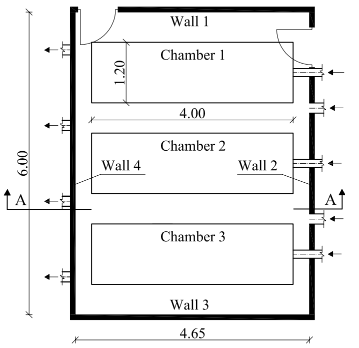

(a) Plan view of pressure chambers.

(b) Construction of pressure chamber.

Figure 2.21. Construction of three pressure chambers above the ceiling. [Chodor and Taradajko, 2013]

The resulting measurements showed that reducing the supply area to only parts of the ceiling significantly reduced the performance of the system, meaning it resulted in high velocities in the room. With the entire ceiling area as supply opening, the system was able to handle the highest heat loads without creating draught in the room. Resulting temperature gradients were very low in all cases. Another interesting observation was that different heat load positions created very different airflow stability in the room. Positioning the heat loads in one end of the room produced a steady, turbulent but high velocity flow in the room. Distributing the heat loads evenly in the room reduced the velocities, however made the velocities less stable. The possible reason for this type of flow was not clarified. The velocity distribution in the room in the mentioned cases are shown in figure 2.22.

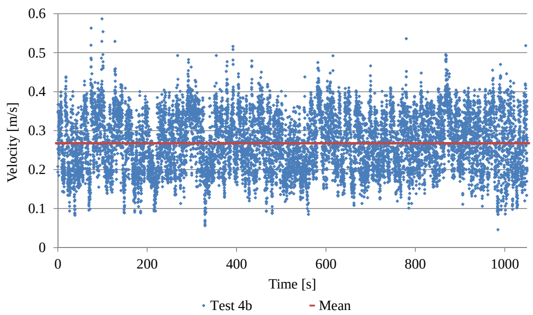

(a) Velocities with heat loads in one end of test room.

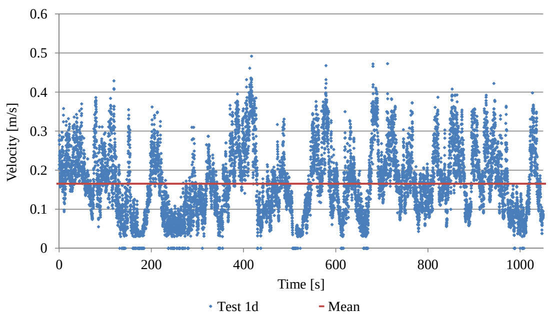

(b) Velocities with heat loads evenly distributed.

Figure 2.22. Velocity over time for different heat load positions. [Nielsen et al., 2010]

Finally, Chodor and Taradajko [2013] also conducted CFD simulations. The predictions showed interesting results regarding room height, namely that velocities in the room increased significantly when increasing room height. Vector plots of two predictions with equal flow rates are shown in figure 2.23 on the facing page.

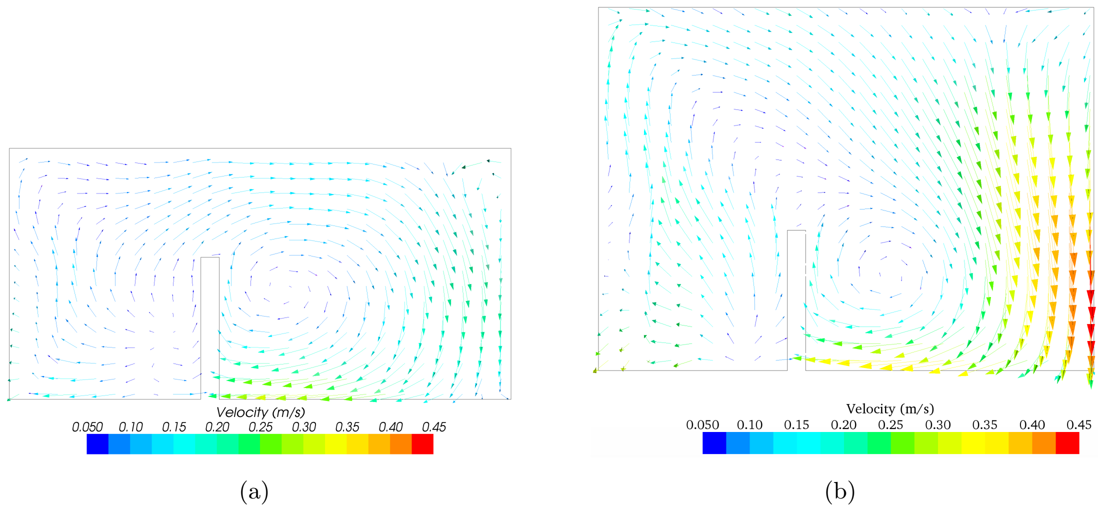

Figure 2.23. CFD prediction with (a) low room height and (b) large room height. [Chodor and Taradajko, 2013]

With large room height, the velocities in the occupied zone were much higher than in the room with a lower room height. It should be mentioned that the CFD simulations did not work out totally as intended but they did however consist with a dimensionless analysis of the measurements also performed by Chodor and Taradajko [2013]. Another thing that is worth to mention is that after Chodor and Taradajko [2013] had finished their thesis, it was discovered that there had been a leakage of the pressure chambers, making all flow rate measurements uncertain to an unknown degree. Therefore the results should be observed with caution.

Design criteria 3

In this chapter the design criteria which are fundamental for the evaluation of measurements and simulations are defined. In this study, only the thermal indoor environment is investigated, thereby neglecting both atmospheric and acoustic environment.

To be able to evaluate the indoor climate, it is important to define the wanted quality of the indoor climate. DS/CEN/CR 1752 [2001] specifies three categories of indoor climate, namely categories A, B and C. It is decided to use category B in these evaluations, mainly because it corresponds to earlier evaluations of diffuse ceiling ventilation and therefore makes it possible to compare experimental results with earlier experiments. Furthermore, fulfilling this category ensures what can be regarded as acceptable indoor climate. In DS/EN 15251 [2007], which uses same categories as DS/CEN/CR 1752 [2001], following explanation of category B is written: "*normal level of expectation ans should be used for new buildings and renovations*". [DS/EN 15251, 2007] Before considering any criteria from category B, the requirements from the Danish Building Regulations, BR [2010], must of course always be fulfilled.

3.1 Thermal comfort criteria

According to BR [2010] buildings must be constructed such that a comfortable and healthy temperature can be maintained in occupied spaces under the intended operational conditions and at appropriate levels of human activity. The thermal indoor climate is evaluated by means of the temperature of the air and surfaces, the air velocity and turbulence intensity of the air. The Danish Building Regulations refer to DS/EN ISO 7730 [2006] for specification of the thermal indoor climate for various types of occupied spaces.

The PMV (Predicted Mean Vote) and PPD (Predicted Percentage Dissatisfied) indexes described in DS/EN ISO 7730 [2006] express the thermal discomfort (warm or cold) of an entire human body, however thermal dissatisfaction can be very local, caused by heating or cooling of individual parts of the body. This is known as local discomfort, and criteria for local thermal discomfort are used to determine the quality of the thermal indoor climate. The most common cause of local discomfort is draught which is evaluated by the local air velocity. Also the local draught rate (DR) is evaluated. Other causes for local discomfort are vertical temperature gradient and radiant temperature asymmetry. The causes for discomfort and their limits for category B are shown in table 3.1 on the next page with respect to actual measurable values.

Mean air velocity [m/s]	Draught rate [%]	VTG [K]	RTA [K]
< 0.19	< 20	< 3	< 5

Table 3.1. Applicable limits for cause of local thermal discomfort for mean air velocity, draught rate (DR), vertical temperature gradient (VTG) and radiant temperature asymmetry (RTA).[DS/EN ISO 7730, 2006]

3.1.1 Mean air velocity

One of the major problems with ventilation is draught. The sensation of draught can be experienced in different ways; as high air velocities and as a combination of air velocity, turbulence intensity and temperature called draught rate (DR). To fulfill the requirements for category B in DS/EN ISO 7730 [2006], mean air velocities should not exceed 0.19 m/s. However, since this study is also interested in experiments conducted in earlier years, comparison with these is interesting. Most experiments with diffuse ceiling ventilation have been evaluated with a mean air velocity limit of 0.15 m/s, which is also the underlying basis of evaluations in this study [Chodor and Taradajko, 2013], [Nielsen, 2007]. Also, the 0.19 m/s are based on a turbulence intensity of 40 % and air temperature equal to the optimal operative temperature. With the possibility of higher turbulence intensity and varying temperatures, the limit of mean air velocity is selected to be 0.15 m/s.

3.1.2 Draught rate

Draught rate (DR) is a combination of local air velocity, turbulence intensity and temperature that takes into consideration that people are more likely to experience draught at low temperatures rather than high. Draught rate is used to describe the percentage of people predicted to feel discomfort caused by draught. The model applies mainly to sedentary activity and predicts the draught rating at neck level. Since draught rate is dependent on both mean air velocity, local turbulence intensity and local air temperature, optimal conditions can allow for an even higher mean air velocity than 0.15 m/s, however also restrict to a lower mean air velocity if conditions are not favorable. Draught rate can be calculated from equation 3.1 and is based on the local turbulence of the air (equation 3.2) which is based on the standard deviation of measured velocities (equation 3.3). [DS/EN ISO 7730, 2006]

$$DR = (34 - t_l)\,(\bar{u}_l - 0.05)^{0.62}\,(0.37 \cdot \bar{u}_l \cdot Tu + 3.14) \tag{3.1}$$

$$Tu = \frac{STD}{\bar{u}_l} \tag{3.2}$$

$$STD = \left(\sum \frac{(u_l - \bar{u}_l)^2}{n-1} \right)^{0.5} \tag{3.3}$$

Where:

DR	Draught rate [%]
t_l	Local air temperature, $20 < t_l < 26$ [°C]
$\bar{u}_l$	Local mean air velocity, $\bar{u}_l < 0.5$ [m/s]
Tu	Local turbulence intensity, $10 < Tu < 60$ [%]
STD	Standard deviation [m/s]
u_l	Local air velocity [m/s]
n	Number of measured values [-]

3.1.3 Vertical temperature gradient

A high vertical air temperature difference between head and ankles can cause thermal discomfort. From category B in DS/EN ISO 7730 [2006] the maximum temperature difference between heights of 0.1 m and 1.1 m, corresponding to the difference between ankles and head for a seated person, should not exceed 3 K/m.

3.1.4 Radiant temperature asymmetry

Radiant asymmetry in the room can be experienced in different ways, either between walls or from floor to ceiling. Since diffuse ceiling in based on a cold supply through ceiling, the difference between ceiling and floor should be checked to make sure it is within the given limitations. Category B in DS/EN ISO 7730 [2006] sets a limit to respectively horisontal and vertical temperature asymmetry of 5 K and 14 K.

3.2 Indoor air quality

The main requirements for indoor air quality (IAQ) is that breathing in the room should not cause any health risk and that the occupants should perceive the air as fresh and comfortable. These conditions are stated in BR [2010] as well as DS/CEN/CR 1752 [2001]. To obtain a good IAQ the minimum ventilation rates should be able to remove the pollution of the air caused by emissions from both occupants and from the building itself. Earlier studies use a minimum flow rate of 10 l/s per person [Nielsen, 2007]. The necessary fresh air supply is calculated from relevant standards and the one giving the largest flow rate is selected as the low limit for flow rate to the room. The selected room type is open-plan office, which in category B has the following requirements and calculated minimum air flow rates. Flow rates are calculated on the assumption that there are six persons in the room and are shown in table 3.2 on the next page.

Standard	Minimum air flow		
	[l/s/person]	[l/(s·m^2)]	[m^3/s]
Previous studies	10*	-	0.060
DS 15251	7	0.7	0.062
BR10	5	0.35	0.040
CN 1752	7	-	0.042

Table 3.2. Minimum supply air flow rates to ensure good indoor air quality. *[Nielsen, 2007]

The above stated minimum flow rates need to be followed in order to maintain an acceptable level of indoor air quality, however in the experiments this does not apply. The design charts created to evaluate the thermal climate in chapter 5 include the minimum allowable flow rate to show the full picture of the cooling capacities.

Experimental set-up 4

Full-scale experiments are carried out in a laboratory at the Department of Civil Engineering at Aalborg University, Aalborg, Denmark. In this chapter the experimental set-up is described. The description includes presentation of the test room, it's boundaries and how the air distribution system works. Next follows a description of the methodology and a detailed walk-through of the measurements being conducted.

4.1 Test chamber

An enclosed test chamber is used in order to conduct full-scale measurements. The chamber is located in a laboratory and has inner dimensions of 4.65 m x 6 m x 4.5 m. The chamber is constructed so that the height of the room can be changed with a maximum room height of 4.4 m. In this height an acoustic ceiling installed as diffuse ceiling, and this ceiling will be used as supply in one of the experiments. The other experiments are conducted with a suspended ceiling in heights of 2.5 m and 4.1 m. Pictures of the room are shown in figure 4.1.

(a) (b)

Figure 4.1. Test chamber from (a) outside and (b) inside.

The internal walls of the test chamber consist mainly of wood. The room has two wooden walls, one wall partly consisting of wood and glass and one wall of plasterboard elements. The floor also consists of wood. Plan and sectional views of the test chamber are shown in figure 4.2 on the next page.

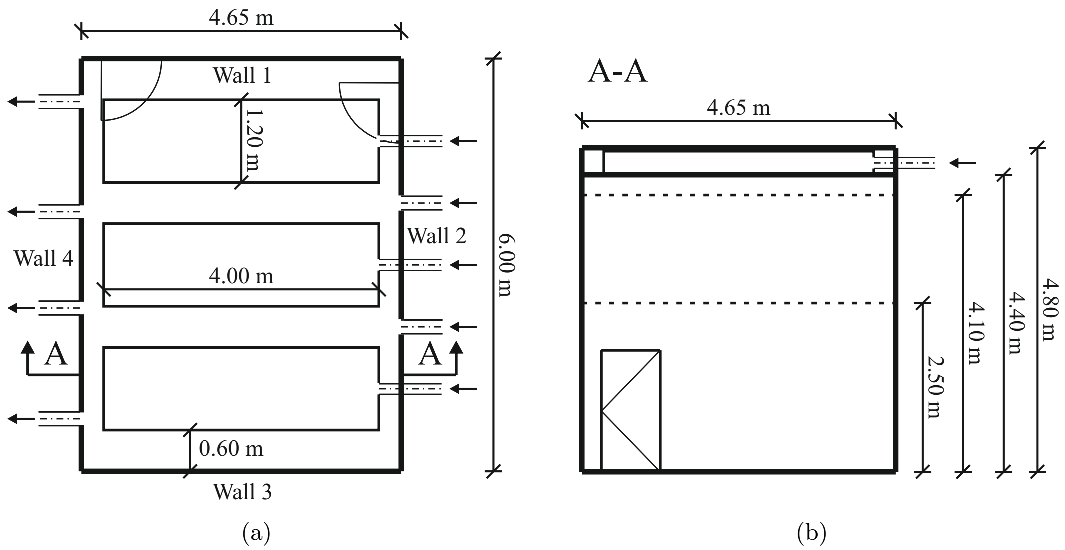

Figure 4.2. (a) Plan view and (b) sectional view of test chamber. Dotted lines indicate the different ceiling heights.

Above the acoustic ceiling are three pressure chambers which can be used to supply air at only parts of the ceiling, however during these experiments the entire ceiling area is used as supply. Pressure is measured in the pressure chambers (and the plenum around the chambers) to ensure an even pressure distribution on the ceiling. The air distribution system is described in Appendix E.

The wooden floor is insulated with 50 mm polystyrene, the walls above the lowest ceiling are insulated with bags containing stone wool (see figure 4.1(a) on the preceding page, and the top of the box is also insulated with bags containing stone wool. The laboratory is tried kept at a constant temperature of 20 °C and during experiments the temperature in the test chamber should be as close to the temperature in the laboratory as possible to keep heat transfer between laboratory and test room at a minimum. Additionally the pressure difference between laboratory and test room is observed, and the inlets and outlets of the air distribution system are regulated to keep this pressure difference at a minimum.

4.1.1 Ceiling construction

Two different types of ceiling is investigated. First, a modular ceiling is tested in two different heights, 2.5 m and 4.1 m. The ceiling consists of quadratic stone wool elements resting on reversed T-profiles of aluminium as shown in figure 4.3 on the next page.

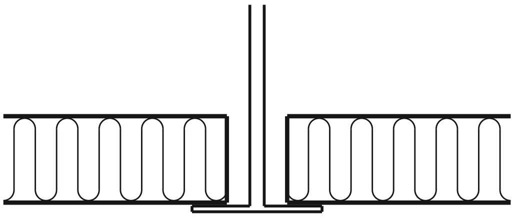

(a) Construction of modular ceiling.

(b) Modular ceiling as installed.

Figure 4.3. Modular ceiling used in heights of 2.5 m and 4.1 m.

Afterwards a homogenous acoustic ceiling in the height of 4.4 m is investigated, to clarify the importance of both room height and supply geometry. The structure of the ceiling and a photo from when it is mounted is shown in figure 4.4.

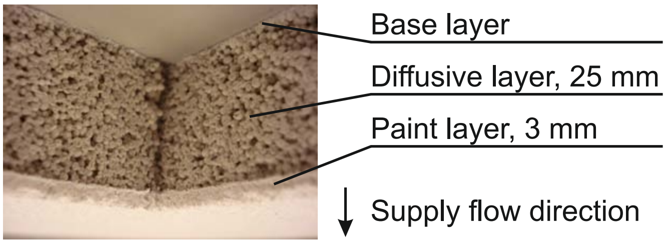

(a) Construction of diffuse ceiling [Chodor and Taradajko, 2013].

(b) View of diffuse ceiling.

Figure 4.4. The acoustic ceiling used in a height of 4.4 m.

4.2 Measurements and methodology

In this section the various measurement equipment is presented, and their specific purpose explained. The main measurements concern temperature and velocity since these parameters are the ones used to evaluate the thermal climate in the chamber. The principle of the occupied zone is explained in section 2.1.1 on page 3 and now the principle is applied to the test chamber. The test chamber is assumed to be surrounded by other rooms, which means the occupied zone will look as shown in figure 4.5 on the following page. [DS/EN 13779, 2007]

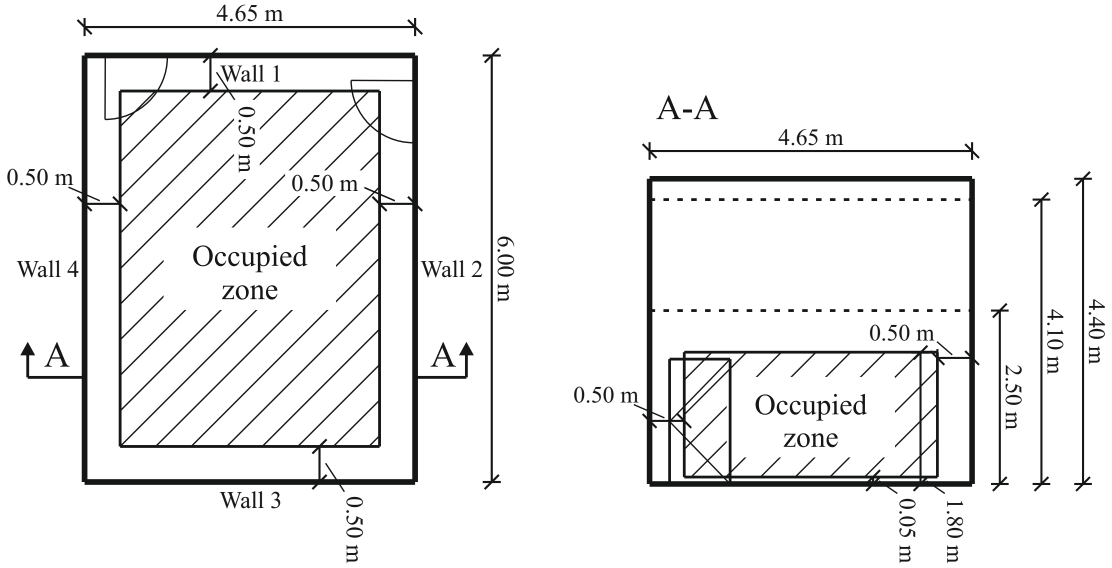

(a) Plan view of occupied zone

(b) Sectional view of occupied zone. Dotted lines indicate the different ceiling heights.

Figure 4.5. The occupied zone in the test room created based on recommendations from DS/EN 13779 [2007].

Some measurements are performed outside the occupied zone, these are not used in the evaluations of the indoor climate, but to understand the airflow taking place in these positions.

To perform the experiments, various equipment needs to be introduced, but first graphic legends of the equipment are shown in table 4.1.

Legend	Description
●	Thermocouple
○	Anemometer
□	Manikin
×	Fixed pole
×	Movable pole in occupied zone
×	Movable pole outside occupied zone

Table 4.1. Legends for various equipment used in the experiments.

Descriptions and positions of the used equipment are explained in the following.

4.2.1 Velocity

The main evaluations regarding the thermal climate in the room deal with the velocities in the occupied zone. The velocity measurements are performed with Dantec hot-sphere anemometers which are described in Appendix C. Since the measurements are conducted in steady state conditions, the maximum velocity measured as an average over 15 minutes is used to evaluate the velocities in the room. Velocities are logged for every 0.1 seconds ensuring a detailed mapping of the velocity over time.

4.2.2 Temperature

Temperature measurements are conducted by use of type K thermocouples which are described in Appendix D. Temperatures are monitored for several reasons, first to control the ongoing conditions, and to evaluate the thermal climate in the room. Furthermore a set of measurements is conducted as an aid to later mentioned CFD investigations, since boundary conditions used in those are obtained from measurements. When monitoring the temperature after changing the set-up or air flow conditions, it is possible to estimate when the system is stabilised. For each experiment temperatures are first stabilised and then logged and averaged over 15 minutes.

4.2.3 Measurement points

Measurements in the room include both temperature and velocity, and the equipment used are attached to movable and fixed poles. The exact locations of equipment in the room are explained in the following.

Movable poles

The movable poles include both thermocouples and anemometers. A picture and a sketch of the movable poles is shown in figure 4.6. For each location of the movable poles, an anemometer and thermocouple is placed in heights of 0.1 m, 1.1 m and 1.7 m. Heights are based on recommendations from DS/EN ISO 7726 [2001] and symbolises ankle, abdomen and neck height for a standing person.

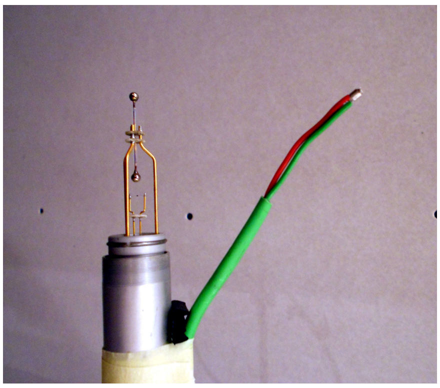

(a) Thick thermocouple and anemometer in a measurement point. The thermocouples have a safe distance of approximately 60 mm from the hot-sphere anemometers.

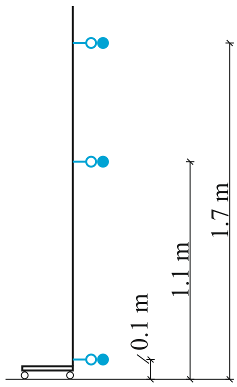

(b) Movable poles with equipment.

Figure 4.6. Movable columns measure both temperature and velocity in three heights.

Measurement points for the movable poles are shown in figure 4.7 on the next page.

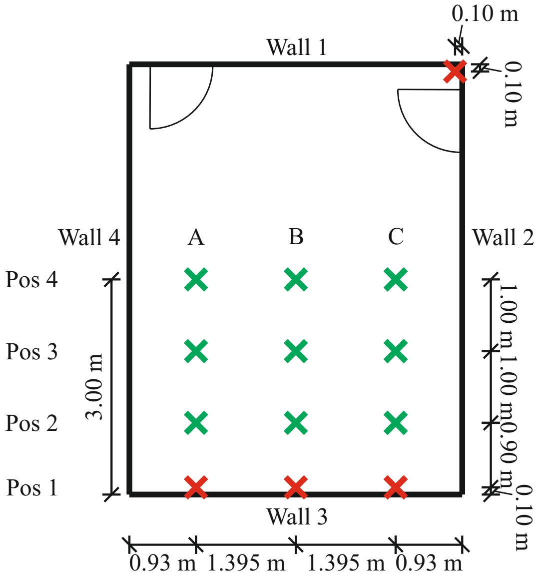

Figure 4.7. Measurement points for each case. Red crosses are outside the occupied zone while green crosses are inside.

The reason the poles do not cover the entire area is due to similarity in the set-up and because they should not be positioned in the vicinity of heat sources because of buoyant flow from the manikins.

Fixed pole

One large fixed pole which covers the entire room height is positioned in the middle of the room. There are only placed thermocouples on the fixed pole to observe the vertical temperature gradient. A sketch and picture of the fixed pole are shown in figure 4.8 on the facing page.

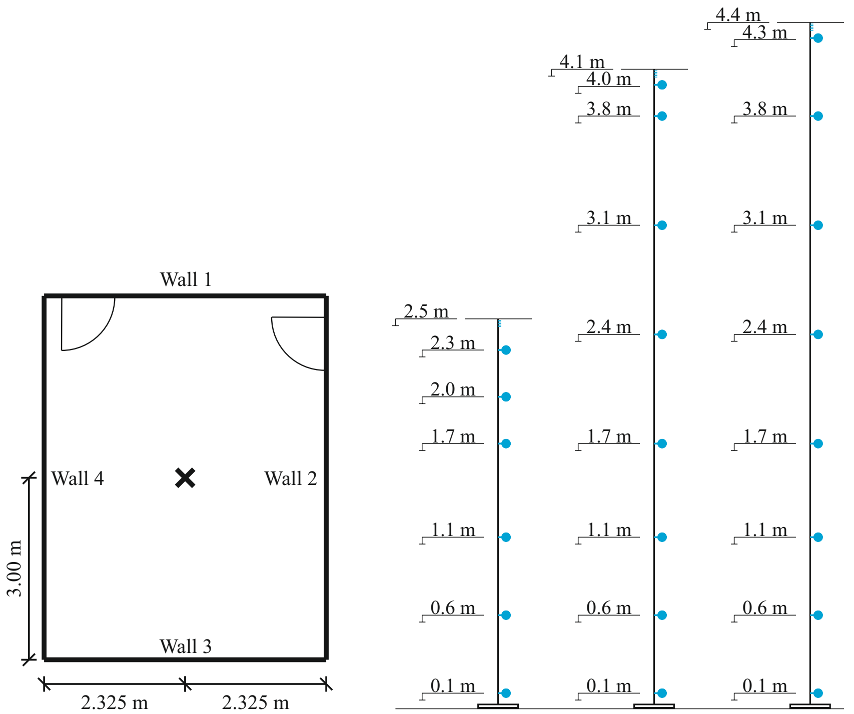

(a) Fixed pole positioned in the middle of the test chamber

(b) The fixed pole is modified between the experiments.

Figure 4.8. Fixed pole in the middle of the room with thermocouples to capture a detailed vertical temperature gradient in the room.

On the topmost part of the fixed pole a set of thin thermocouples is placed with 10 mm difference. This is done to get a detailed view of the vertical temperature gradient very close to the ceiling to see what happens in this region and also to spot what differences are between the two different supply geometries. A sketch is shown in figure 4.9.

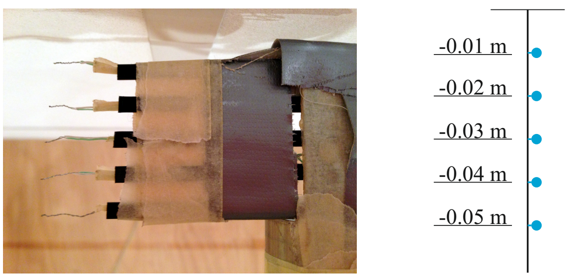

(a)

(b)

Figure 4.9. The set of thin thermocouples is in all cases positioned 10 - 50 mm from the ceiling.

Additional temperature measurements

To monitor the surface temperatures in the room, two thin thermocouples are positioned on every surface. The thermocouples are covered in thermal paste and taped to the wall. Thermal paste conducts heat very well, so adding it should enhance the connection between thermocouple and wall. Surface temperature serve the purpose as boundary conditions in the CFD simulations which are introduced in chapter 6.

For floor and ceiling, the positions of thermocouples are shown in figure 4.10.

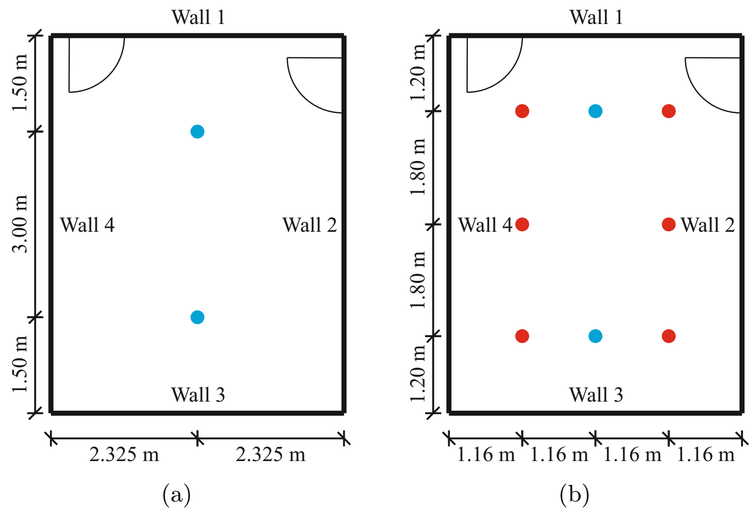

Figure 4.10. Thermocouples taped to (a) floor and (b) ceiling. Blue ones on the ceiling surface, red ones are just above ceiling.

When using the modular ceiling, the thin thermocouples are positioned just on top of the ceiling modules to capture the inlet temperature as well as possible. With diffuse acoustic ceiling it is not possible to place them on top of the ceiling, so they are distributed over the bottom side of the ceiling. This rules them out of measuring a supply temperature that is trustworthy.

The position of thermocouples on the walls change when testing different room heights. The three different situations are shown in figure 4.2(b) on page 24. Thermocouples on walls 1 and 3 have identical positions, and thermocouples on walls 2 and 4 have identical positions, and are shown in figure 4.11. When changing between room heights of 4.1 m and 4.4 m, the thermocouples do not change position.

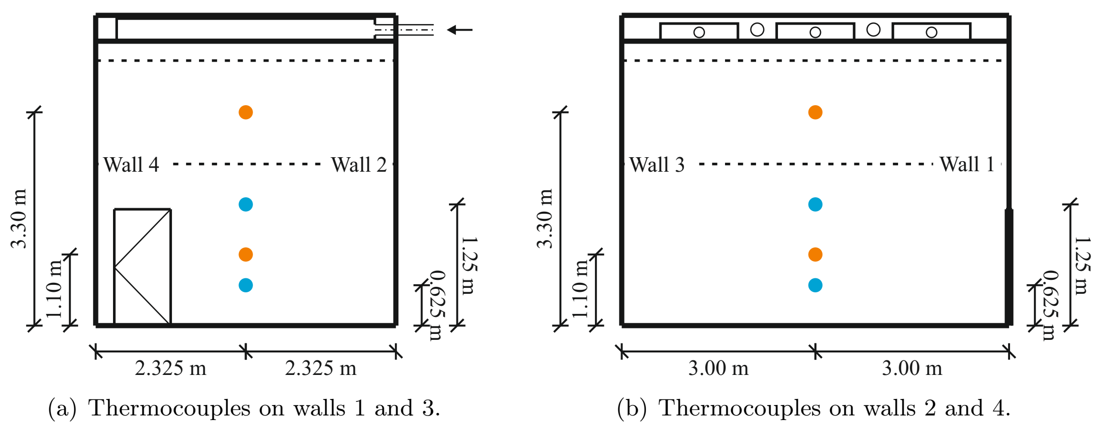

Figure 4.11. Blue indicates positions with ceiling at a height of 2.5 m while orange indicates positions with ceiling at 4.1 m and 4.4 m.

Thermocouples are positioned in several other positions outside the boundaries of the test room which are shown in appendix B.

4.3 Test conditions

In this section the experimental set-up is explained, and all test-cases described.

4.3.1 Heat sources

In all test cases, six thermal manikins are used as heat loads to the room. Three different types of manikins are used, and pictures of these are shown in figure 4.12.

(a) (b) (c)

Figure 4.12. Different shapes of manikins used as heat loads in the experiments.

Each manikin is set release heat corresponding to a person doing sedentary activity at a metabolic rate of 1.2 met. Only free heat is considered, meaning convective and radiative energy. For the given activity level the free heat release corresponds to 77 W per manikin [Hyldgård et al., 1997]. Please note that even though the manikins have shape and heat release as a person, they should not be limited to only be perceived as persons, but as heat sources in general. In order to give each manikin as even an amount of power as possible, two transformers each controlling three manikins are used, and figuratively shown in figure 4.13. A quick test showed a very even distribution of the available power between the manikins.

Figure 4.13. The two transformers, each supplying power to three manikins.

For each ceiling height, three different heat load distributions are investigated. This is done to better understand the importance of the positions of the heat loads when using diffuse ceiling ventilation. The different positions are shown in figure 4.14. Specific positions are shown in figures B.2, B.3 and B.4 in Appendix B.

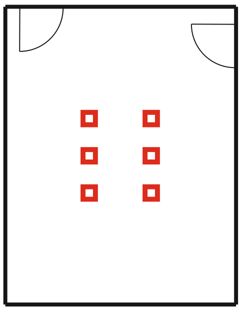

(a) Centered (Position 1)

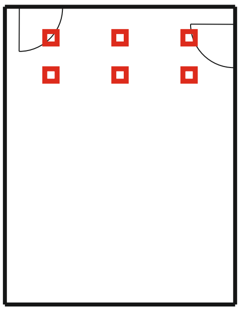

(b) In one end (Position 2)

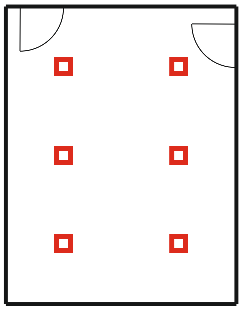

(c) Evenly distributed (Position 3)

Figure 4.14. The three different heat load distributions.

Pictures of two of the three positions are shown in figure 4.15.

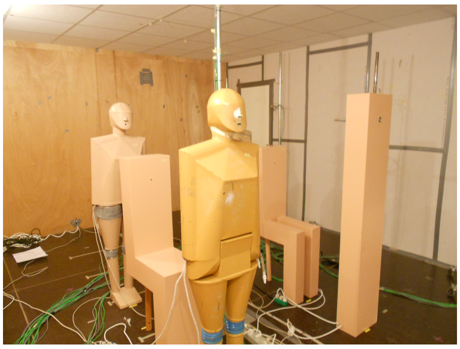

(a) Centered (Position 1).

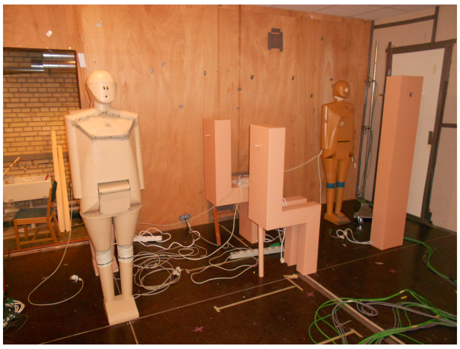

(b) In one end (Position 2)

Figure 4.15. Heat load positions 1 and 2. With evenly distributed manikins they have the same mutual position as in position 1 but naturally located as shown in figure 4.14(c).

The reason for testing these three specific heat load positions is to try to understand what influence the position has on the thermal climate and flow pattern in the room. These heat loads and their positions are tangible and easy to replicate if necessary.

4.3.2 Test cases

Several variables are changed between the individual experiments. Three different heat load positions, three different ceiling heights including different ceiling geometries. To get an overview of the performance of the system with regard to thermal comfort, several different test conditions for each experiment $(q_0, \Delta T_0)$ are investigated. The power supplied to the manikins is kept constant at 77 W per manikin.

Test cases with same room geometry (room height) are grouped together. Secondly same heat load position are grouped together. These cases are numbered individually, while changes in $(q_0, \Delta T_0)$ are showed by letter. In other words the test case with 2.5 m ceiling, manikin position 1 and lowest flow rate q_0 will is named case 1a. For all experiments, the air is supplied through the entire ceiling surface. Generally, there are nine different test cases, and they are shown in table 4.2.

Case	Heat load		Ceiling height	Ceiling type	Heat load position
	[W]	[W/m^2]	[m]	[-]	[-]
1	468	16.8	2.5	Modular ceiling	Centered
2	468	16.8	2.5	Modular ceiling	In one end
3	468	16.8	2.5	Modular ceiling	Evenly distributed
4	468	16.8	4.1	Modular ceiling	Centered
5	468	16.8	4.1	Modular ceiling	In one end
6	468	16.8	4.1	Modular ceiling	Evenly distributed
7	468	16.8	4.4	Diffuse acoustic ceiling	Centered
8	468	16.8	4.4	Diffuse acoustic ceiling	In one end
9	468	16.8	4.4	Diffuse acoustic ceiling	Evenly distributed

Table 4.2. Different test cases. For each case, several tests are conducted.

Within each test case, various supply flow and corresponding temperature difference $(q_0, \Delta T_0)$ is tested to ensure that a variety of possible situations are covered. The maximum velocity measured in each test case from table 4.2 is used to evaluate the ability of the system to remove heat without creating draught in the occupied zone.

Experimental results 5

In this chapter the most interesting experimental results are presented and analysed, and conclusions to the earlier mentioned problem statements are made. First a study about whether or not it is fair to use similarity principle based on dimensionless numbers is conducted. On basis of that, design charts are created from the results of measurements. Air flow and temperature distribution, stability of air velocity for the various cases are analysed followed by a short analysis of other indoor climate parameters.

5.1 Archimedes number and similarity principle

Archimedes number is used to determine the limiting curves of the air distribution system. It is assumed that any dimensionless velocity in the test room can be given as a function of the Archimedes number under the requirement that the flow is fully developed turbulent flow. It is characteristic for fully developed turbulent flow that a high Reynolds number is present, i.e. the flow in the room is independent on the Reynolds number. [Nielsen, 2007] As an introduction to the main experiments, a test was conducted to verify if the above mentioned is in fact a valid assumption.

In section 2.1 on page 3 the creation of design chart was explained and one of the main assumptions was that the limiting points in the design chart could be based on equation 5.1.

$$\mathrm{Ar} = func\left(\frac{\Delta T_0}{q_0^2}\right) = const \tag{5.1}$$

Observing equation 5.1, second order polynomials can be determined for all flow situations, each individually characterised by a given $\Delta T_0/q_0^2$ ratio; an Archimedes number simplified by having constant geometry. Shown in figure 2.5 on page 8, this ratio is constant in every point along the curve.

In order to test whether or not this method is applicable, first a suitable Archimedes number is selected. By suitable meaning an Archimedes number for which a series of measurements can be conducted under applicable conditions. Figure 5.1 on the following page shows five different curves for constant Archimedes number. The shown test is only performed for the suspended ceiling in a height of 4.1 m.

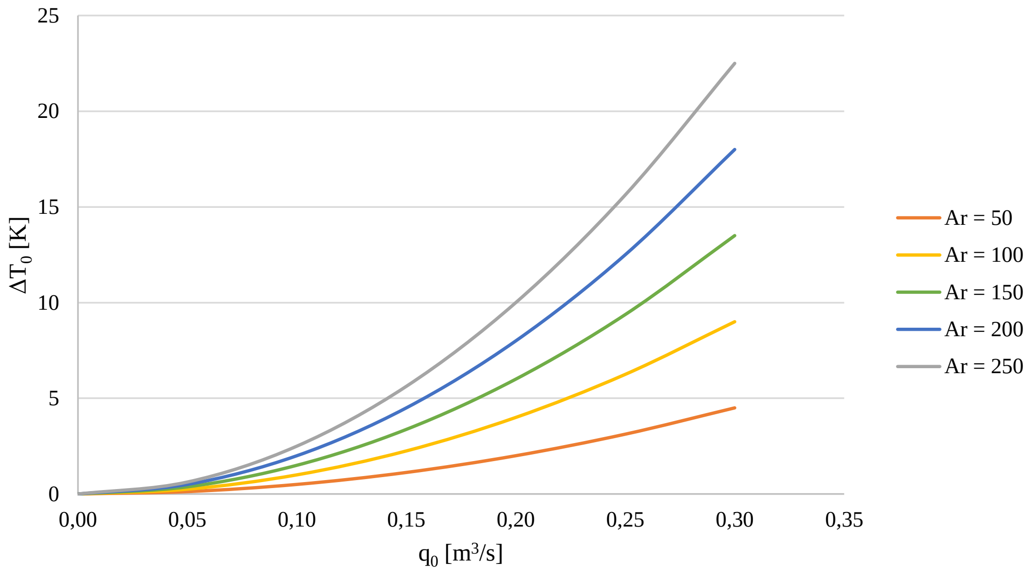

Figure 5.1. Curves on a ΔT_0-q_0 chart. Every point along the individual curves correspond to a constant value of $\Delta T_0/q_0^2$ which is also a constant Archimedes number.

The curves above are theoretical, and the following experiment is then to investigate whether or not the similarity principle is applicable; that any dimensionless velocity u_{OCZ}/u_0 is constant along such curve. First the measurement conditions need to be tested, and to do so, the curve for an Archimedes number of 150 is selected. To obtain the required measurements, the heat load to the room, along with flow rate (and therefore also temperature difference) need to be varied. The heat load is calculated from equation 5.2 on page 40 from first having set $\Delta T_0/q_0^2$ constant at 150 and yield the following measurement conditions shown in table 5.1. Heat load varies between 83 W and 4059 W.

Case	q_0 [m^3/s]	$\Delta T_{\text{theoretical}}$ [K]	$\Delta T_{\text{measured}}$ [K]	Heat load [W]
a	0.077	0.89	0.98	83
b	0.137	2.81	3.22	465
c	0.200	5.99	6.24	1450
d	0.282	11.89	11.75	4059

Table 5.1. Measured conditions for verification of similarity principle.

During measurements it was attempted to keep the temperature in the test room as close to the temperature in the laboratory, however since the laboratory temperature is difficult to keep stable, small differences occurred. The resulting graphs for theoretical and measured polynomial curves are shown in figure 5.2 on the next page. A trend line is added to the measured values to verify their correlation with the theoretical polynomial.

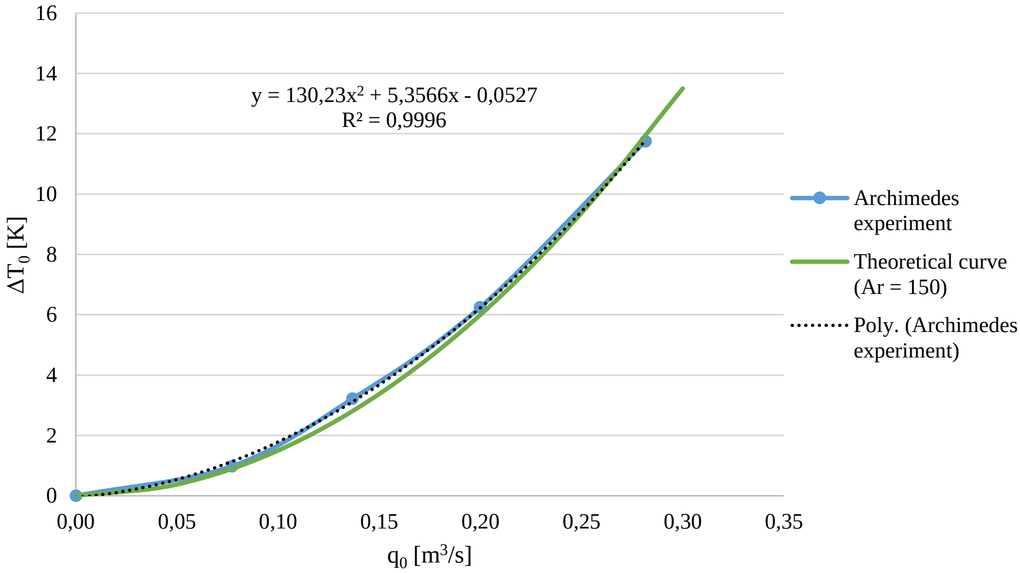

Figure 5.2. Comparison of theoretical and experimental curves with constant Archimedes number.

Figure 5.2 shows a very good correlation between theoretical and measured values. The Archimedes number is constant, or at least very close to constant, along the shown curve. At very low heat loads the flow in the room would more likely be laminar rather than turbulent, or at least dependent on the Reynolds number.

To verify the theory that any dimensionless velocity can be given as a unique function of the Archimedes number, the dimensionless velocity in the occupied zone is also tested. With a constant Archimedes number, the maximum dimensionless velocity should be similar in the four measured cases. Heat loads are positioned in one end of the room and measuring points are the ones explained in figure 4.7 on page 28. The resulting dimensionless velocities are shown in table 5.2. Supply velocity is calculated from equation 2.3 on page 7.

Case	q_0 [m^3/s]	a_0 [m^2]	u_0 [m/s]	$u_{\max}$ [m/s]	$u_{\max}/u_0$ [-]
a	0.077	27.9	0.002764	0.108	39.08
b	0.137	27.9	0.004903	0.223	45.49
c	0.200	27.9	0.007161	0.347	48.45
d	0.282	27.9	0.010092	0.526	52.12

Table 5.2. Dimensionless velocities in the occupied zone.

The table shows that when keeping a constant Archimedes number, the dimensionless velocities do not stay constant when changing test conditions. The dimensionless velocity increases slightly when increasing flow rate, at least when the heat loads were positioned in one end of the room. This will be investigated further in the next sections when three different heat load positions are tested. Observing table 5.2 the dimensionless velocities seem to vary quite a lot, but one should take into consideration that these are based on a rather huge supply area of 27.9 m^2. If the dimensionless velocities were tested with a smaller supply area, the changes would be much smaller. There is no doubt though, that the dimensionless velocities in the occupied zone to some extend increase when increasing flow rate.

The measurements showed that the dimensionless velocity was not totally constant along the curve shown in figure 5.2 on the previous page, however the changes were not very large. Equation 5.1 on page 35, which is fundamental in the creation of design graphs in the following section, is still used, but as a precaution, several measurements for each case is conducted.

5.2 Experimentally obtained data

The data in this section is obtained in order to evaluate what effect position of heat loads, room size and supply geometry have on the air velocities and temperatures in the test room.

A collection of air flow rates, temperatures and maximum measured velocities for all measured cases are shown in the following tables. In table 5.3 the results from the experiment with room height of 2.5 m are shown, table 5.4 on the facing page shows the results from having a ceiling height of 4.1 m and table 5.5 on the next page shows the results from having the full available height of the room, 4.4 m.
The inlet temperature is measured in the supply ducts as shown in section 4.2 on page 25, which is also fairly close to the actual supply to the room.

Case	q [m^3/s]	t_s [°C]	t_e [°C]	ΔT_0 [K]	t_{ocz} [°C]	t_{lab} [°C]	ΔT_{lab} [K]	u_{max} [m/s]
1a	0.055	11.22	20.37	9.15	20.49	19.91	0.58	0.106
1b	0.107	14.70	19.77	5.07	19.89	19.88	0.01	0.111
1c	0.179	16.60	19.78	3.18	19.96	20.46	0.50	0.117
2a	0.055	11.04	20.40	9.36	20.44	19.87	0.57	0.149
2b	0.107	14.70	19.77	5.07	19.81	19.82	0.01	0.159
2c	0.179	16.59	19.60	3.01	19.63	20.13	0.50	0.181
2d	0.264	17.79	20.03	2.24	20.05	20.66	0.62	0.205
2e	0.312	18.70	20.34	1.63	20.35	20.59	0.24	0.201
2f	0.035	8.86	20.35	11.48	20.44	19.81	0.63	0.138
3a	0.055	11.03	20.16	9.13	20.30	19.85	0.45	0.084
3b	0.107	14.68	19.66	4.98	19.77	19.81	0.04	0.102
3c	0.179	16.60	19.70	3.11	19.73	20.28	0.55	0.097

Table 5.3. Resulting temperatures and maximum velocities from the experiments conducted with room height of 2.5 m.

Case	q [m^3/s]	t_s [°C]	t_e [°C]	ΔT_0 [K]	t_{ocz} [°C]	t_{lab} [°C]	ΔT_{lab} [K]	u_{max} [m/s]
4a	0.058	11.25	20.26	9.01	20.45	19.53	0.91	0.141
4b	0.113	18.50	22.37	3.87	22.46	22.66	0.20	0.147
4c	0.193	20.83	23.35	2.53	23.42	23.95	0.53	0.170
4d	0.292	21.31	22.63	1.31	22.74	22.88	0.14	0.174
5a	0.058	11.20	20.14	8.94	20.30	19.17	1.13	0.195
5b	0.113	19.07	22.56	3.49	22.64	22.90	0.26	0.225
5c	0.193	20.95	23.14	2.19	23.12	23.72	0.60	0.232
5d	0.292	20.62	22.62	2.00	22.76	22.99	0.23	0.254
6a	0.058	11.23	20.14	8.90	20.29	19.33	0.96	0.104
6b	0.113	18.51	22.51	4.01	22.58	22.80	0.22	0.130
6c	0.193	20.25	23.10	2.86	23.11	23.66	0.55	0.190
6d	0.292	21.31	22.67	1.36	22.75	23.12	0.37	0.186
6e	0.271	20.33	21.44	1.11	21.54	21.36	0.18	0.136
6f	0.076	13.73	19.35	5.63	19.45	18.95	0.50	0.164

Table 5.4. Resulting temperatures and maximum velocities from the experiments conducted with room height of 4.1 m.

Case	q [m^3/s]	t_s [°C]	t_e [°C]	ΔT_0 [K]	t_{ocz} [°C]	t_{lab} [°C]	ΔT_{lab} [K]	u_{max} [m/s]
7a	0.064	9.66	19.56	9.90	19.57	19.82	0.26	0.136
7b	0.117	15.03	19.37	4.34	19.42	20.09	0.67	0.145
7c	0.201	17.10	19.81	2.72	19.90	20.85	0.95	0.162
7d	0.296	18.87	20.42	1.55	20.55	20.80	0.25	0.153
8a	0.064	9.71	19.44	9.73	19.39	19.79	0.40	0.224
8b	0.117	14.94	19.16	4.21	19.14	19.87	0.74	0.239
8c	0.201	17.12	20.08	2.96	20.09	21.35	1.25	0.250
8d	0.296	18.98	20.83	1.85	20.84	21.88	1.04	0.268
9a	0.064	9.68	19.52	9.83	19.52	19.81	0.29	0.183
9b	0.117	14.99	19.28	4.29	19.24	20.01	0.77	0.152
9c	0.201	17.13	19.91	2.78	19.93	21.05	1.12	0.200
9d	0.296	19.05	20.59	1.54	20.64	21.14	0.50	0.198

Table 5.5. Resulting temperatures and maximum velocities from the experiments conducted with room height of 4.4 m.

5.3 Design charts for different set-ups

The obtained results for flow rate and velocities are used in the creation of design graphs for the different cases, however to be able to compare the different cases, also with earlier experiments, ideal conditions should be utilised. This means that temperatures measured for supply and extract are not used in the creation of design graphs, but rather in the evaluation of the thermal indoor climate.

The calculation of the temperature difference in case of all heat being removed by the ventilation at a certain heat load is shown in equation 5.2.

$$\Delta T_0 = \frac{\Phi}{\rho \cdot c_p \cdot q_0} \tag{5.2}$$

Where:

ΔT_0	Temperature difference between supply and return flow [K]
Φ	Heat load [W]
c_p	Heat capacity of supply fluid (air) [J/kg K]
q_0	Volume flow rate [m^3/s]

The design charts are based on the theory explained in section 2.1 on page 3 and detailed calculations can be found on the Appendix CD. It was explained that the design chart could be based on both vertical temperature difference and maximum velocities in the occupied zone. This is true, however a temperature gradient was almost not present in the experiments, so it is chosen to create design charts of the system based only on a maximum velocity in the occupied zone of 0.15 m/s. This corresponds to the draught limit in a category B building and enables for comparison with earlier experiments [DS/CEN/CR 1752, 2001].

Theoretically, only one single measurement needs to be conducted for a given case, and the resulting set of (q_0,ΔT_0) can be extrapolated based on the assumption that the product of q_0 and ΔT_0 (the thermal load) is constant for a given case [Nielsen, 2007]. When conducting several measurements per case, the following graphs are created based on a mean product of q_0 and ΔT_0 for the set of measurements.
In the following sections design charts are created for the three different ceiling types, and the three different heat loads positions are evaluated for each ceiling height. Next, a full comparison of the three ceiling types is conducted followed by a comparison with earlier measurements. In this section only the highest velocities in the occupied zone are considered. Further and more detailed interpretation follow in the ensuing sections.

5.3.1 2.5 m modular ceiling

Based on the conducted experiments with a room height of 2.5 m, a design chart showing the limits of the air distribution system for the different heat load positions is shown in figure 5.3.

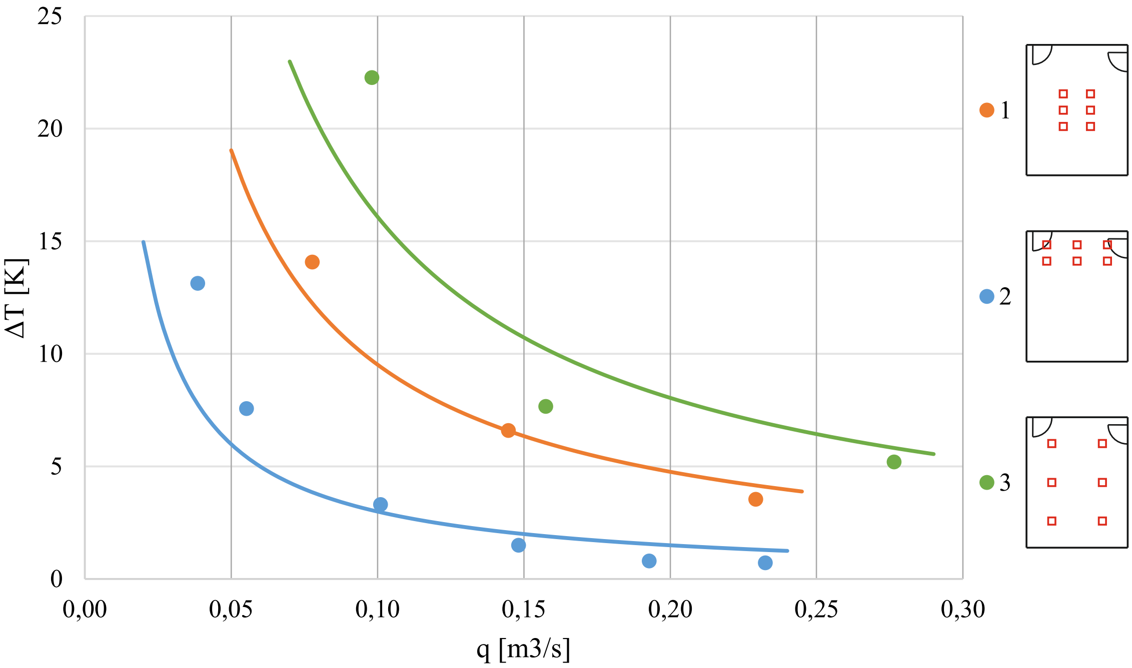

Figure 5.3. Design chart for measurements with modular ceiling in height of 2.5 m.

As expected, with heat loads positioned in one end of the room (Case 2), the highest velocities were measured. Case 3 with evenly distributed heat loads gave the lowest velocities and thereby the highest cooling capacity. The curves are created from a mean product of the limiting (q_0,ΔT_0). Individual measurements deviate slightly from this mean product.

Looking at the system's ability to remove heat in the three cases, the cooling capacity for each case is calculated also from the mean product of q_0 and ΔT_0 giving cooling capacities as shown in table 5.6.

Case	Cooling capacity	
	[W]	[W/m^2]
1	1154	41
2	363	13
3	1950	70

Table 5.6. Cooling capacities for cases 1, 2 and 3.

Both figure 5.3 and table 5.6 indicate that the position of heat sources have a great significance on the cooling capacity of the system.

5.3.2 4.1 m modular ceiling

Next up was the same ceiling geometry as in cases 1, 2 and 3, however in a height of 4.1 m. This was done to test if the room height had a big influence on the cooling capacity. The resulting design graphs for cases 4, 5 and 6 are shown in table 5.4.

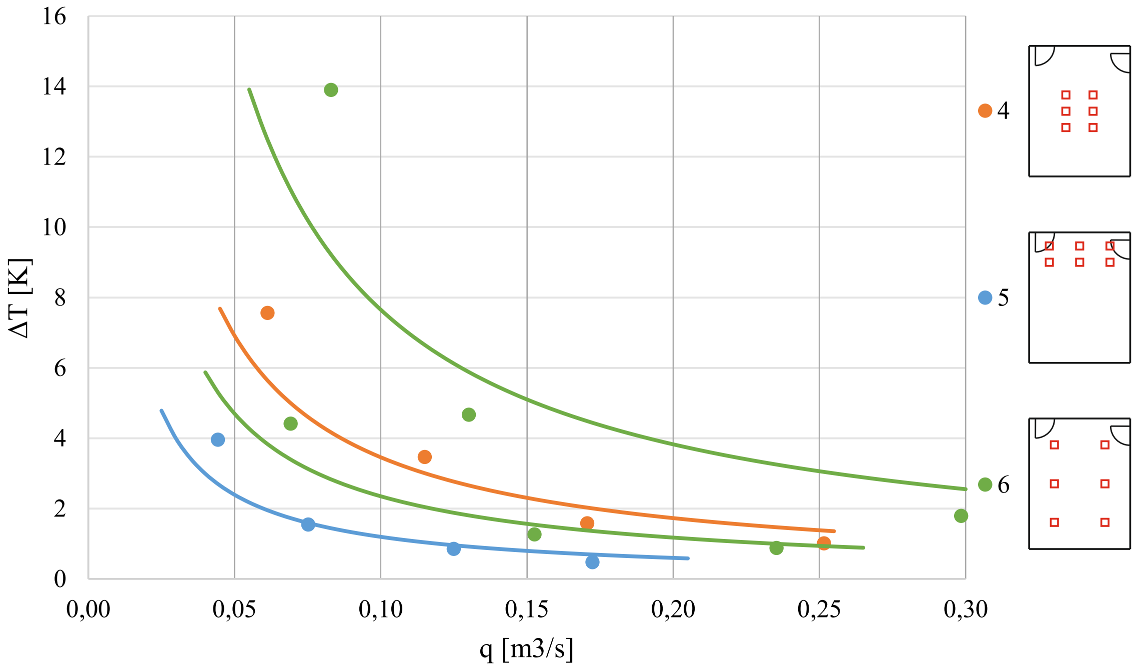

Figure 5.4. Design chart for measurements with modular ceiling in a height of 4.1 m.

Looking at figure 5.4 it might seem odd that there are two different curves for case 6. This is not coincidental. While running measurements for case 6 the resulting maximum velocity changed a lot within the individual experiments. Actually a tendency occurred, that the maximum velocity was in the region of either 0.18 m/s (solid line) or 0.13 m/s (dotted line). This could indicate, as Chodor and Taradajko [2013] also suggested, that the flow in the room does not reaches a steady state condition, but varies between two or more flow solutions. In an air distribution system design phase, naturally the solid line graph should be chosen.

Say the highest graph for case 6 is neglected, the situations vary from a room height of 2.5 m, it is no longer the evenly distributed heat load but the one centered in the middle of the room that gives the highest cooling capacity. This along with the changing velocities in case 6 is discussed further in section 5.4 on page 46. Compared to a ceiling height of 2.5 m the cooling capacities are significantly lower as shown in table 5.7.

Case	Cooling capacity	
	[W]	[W/m^2]
4	419	15
5	145	5
6_1	927	33
6_2	285	10

Table 5.7. Cooling capacities for cases 4, 5 and 6.

5.3.3 4.4 m diffuse acoustic ceiling

The final set of measurements were conducted with the homogenous acoustic ceiling in a height of 4.4 m. The purpose of including this experiment was to investigate the importance of having a different supply geometry, explained in detail in section 4.1 on page 23. The resulting design graphs are shown in figure 5.5.

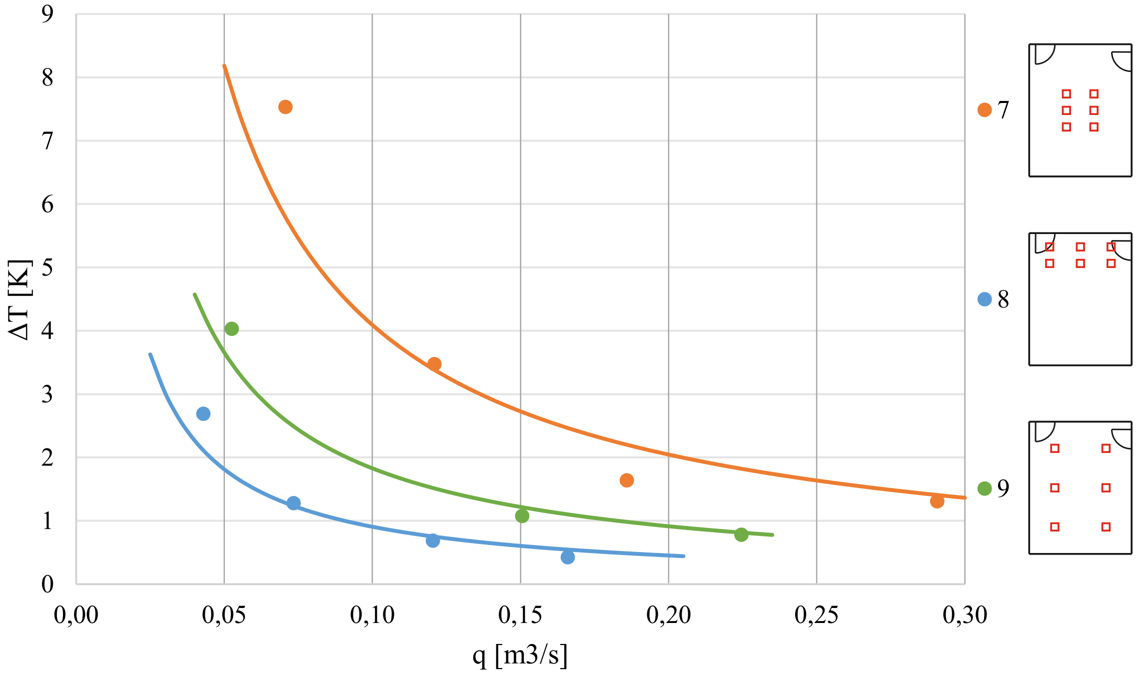

Figure 5.5. Design chart for measurements with acoustic diffuse ceiling in a height of 4.4 m.

As in the situation with room height of 4.1 m, the situation with heat loads in the center of the room gave the highest cooling capacity. One measurement point from case 9 is neglected, because the maximum velocity was much lower than for the other individual measurements. Increasing the flow rate had a very low influence on the resulting velocities in cases 7 and 9, but increased the measured velocities in case 8. It has been characteristic for all measurements having heat loads in one end, that the velocities in the occupied zone increased slightly when increasing flow rate. The cooling capacities for a ceiling height of 4.4 m are shown in table 5.8.

Case	Cooling capacity	
	[W]	[W/m^2]
7	496	18
8	110	4
9	277	10

Table 5.8. Cooling capacities for cases 7, 8 and 9.

Generally the cooling capacities are very similar for room heights of 4.1 and 4.4 m and much higher with room height of 2.5 m, indicating that it is the room height rather than the supply geometry that influences the cooling capacity. The results also show that the position of heat load is very important.

5.3.4 Comparison of design charts

A comparison of the three different room geometries is shown in figure 5.6.

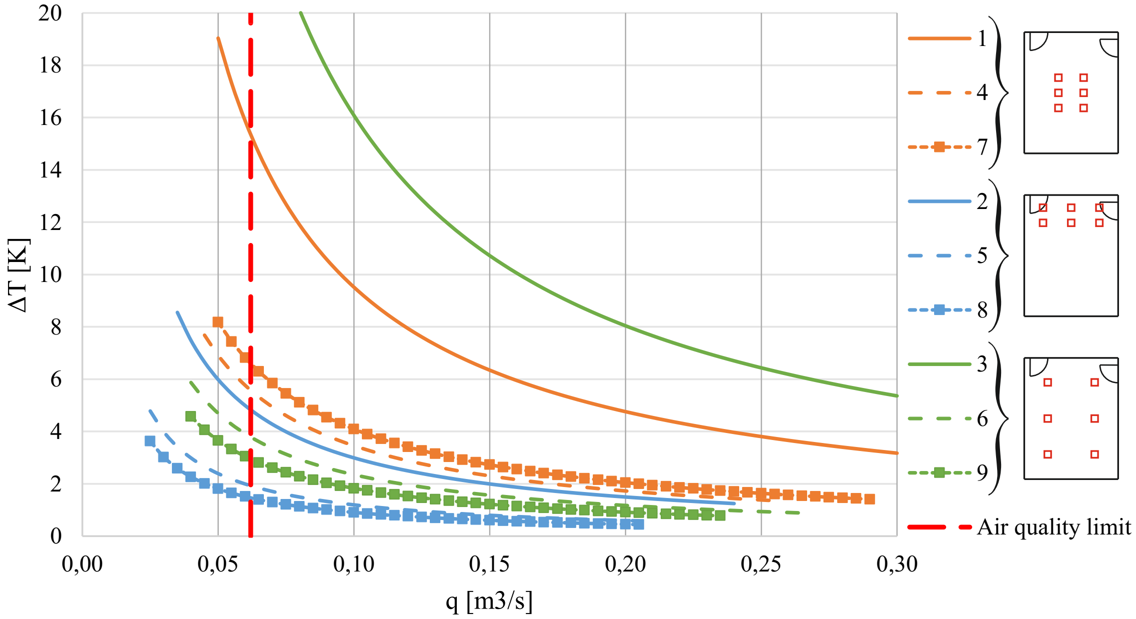

Figure 5.6. All the experiments shown in one chart. Cases 1, 2 and 3 are with room height of 2.5 m, cases 4, 5 and 6 are with room height of 4.1 m and cases 7, 8 and 9 are with room height of 4.4 m.

As already explained and now visualised, the two situations with large room height have much lower cooling capacity than with lower room height. Room heights of 4.1 m and 4.4 m yield quite similar results for heat loads evenly distributed or in one end of the room. This is consistent with the theory about increasing room height increases velocities, however with heat loads in the center of the room, the room height of 4.4 m gives better conditions than 4.1 m.

5.3.5 Comparison with earlier experiments

A comparison with experiments of various diffuser types conducted by Nielsen [2007] is made. Resulting design graphs are plotted together in figure 5.7 on the next page.

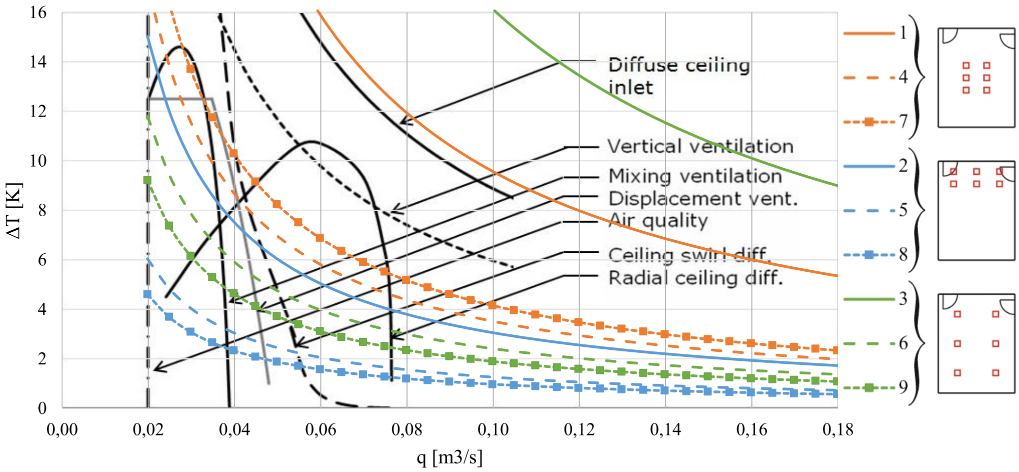

Figure 5.7. Measurements compared to earlier experiment conducted by Nielsen [2011].

With a ceiling height of 2.5 m, the results for diffuse ceiling look similar to ones conducted by Nielsen [2007]. When increasing ceiling height, in this comparison, diffuse ceiling ventilation is less efficient than the other types of air distribution systems presented.

As mentioned in 2.2.3 on page 15, Chodor and Taradajko [2013] made experiments in the same test facility with the same acoustic ceiling as undersigned have conducted experiments with at a height of 4.4 m. Back then, both manikins and light bulbs were used as heat sources (light bulbs positioned high up in the room and close to walls 2 and 4) for which reason the supplied heat loads were much higher. A comparison of heat loads in different positions are shown in figure 5.8.

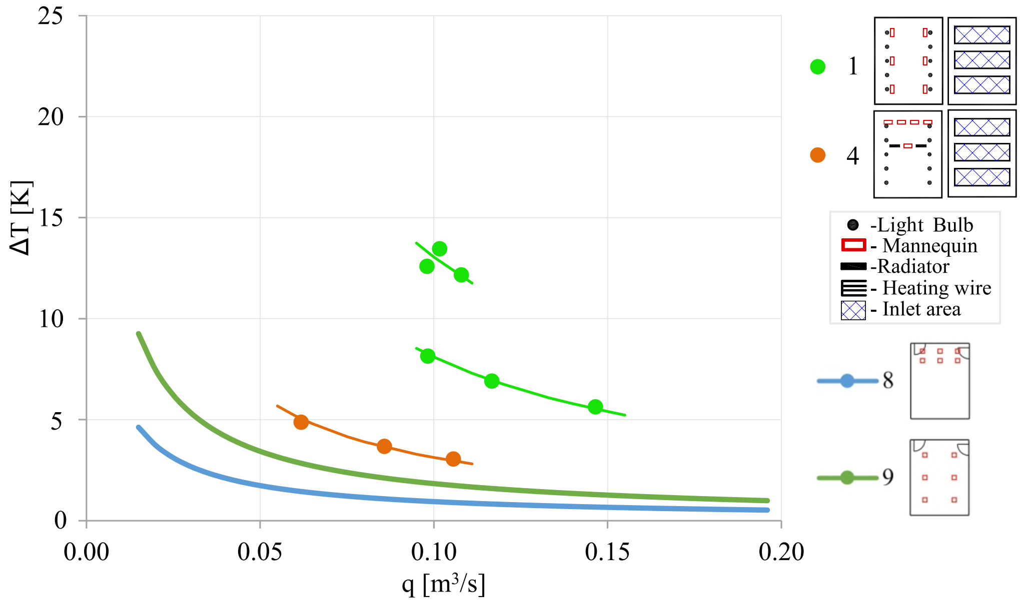

Figure 5.8. Measurements compared to earlier experiment conducted by Chodor and Taradajko [2013].

The results show that Chodor and Taradajko [2013] experienced a larger cooling capacity when having heat loads in more or less same positions. This comparison may not be totally fair because various types of heat loads and always more or less evenly light bulbs activated, but this was the general situation in their experiments. The results also show a significant difference when changing heat load position.

5.4 Airflow distribution

In this section the air flow distribution in different situations is analysed, both with regard to general flow pattern and where in the room the highest velocities occur. Furthermore, since velocities were measured over time, their stability and turbulent behavior is discussed.

5.4.1 Smoke experiments

Smoke experiments were conducted to show the air movement in the test room with varying heat load positions. In most cases it was very difficult to document the flow movements by photos but instead, a drawing is made to visualise the flow directions in the given situations.

Flow through suspended ceiling

Depending on the type of ceiling, flow enters the room in different ways. With the diffuse acoustic ceiling, the entire ceiling construction is semi-homogenous, giving an even air distribution through the ceiling. With the suspended modular ceiling, quadratic stone wool elements are resting on top of reversed aluminium T-profiles. The ceiling modules are not very heavy and not very permeable, so a large part of the air was expected to go through the small slots between the T-profiles and the ceiling elements. Smoke experiments shown in figure 5.9 reveal that this is in fact the case with the suspended ceiling. Smoke was supplied above the suspended ceiling showing how the air enters through the small slots.

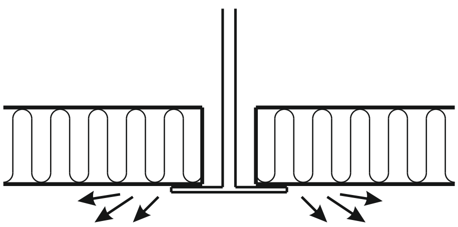

(a) Construction of suspended ceiling.

(b) Smoke entering room through small slots.

Figure 5.9. The construction of suspended ceiling smoke experiment showing the air entering through the small slots.

Jakubowska [2009] made a pressure test to see if there was any pressure differences from having an entire modular ceiling and just one ceiling element. The result was that the pressure difference over one ceiling element was almost 10 times larger than over the entire ceiling at a given flow rate (naturally reduced so the flow rate per area was the same), supporting the theory about a most of the air going through the small slots.

With air passing through the small slots and entering the room at high velocity, some mixing is created close to the ceiling. With the diffuse acoustic ceiling it is different, since the construction is more homogenous and it was expected that the air penetrated the ceiling more or less evenly over the entire ceiling area. This however was impossible to observe in smoke experiments. Following figures show the air movement observed when conducting smoke experiments. Notice that the shown flow patterns were what could be safely concluded from the smoke experiments.

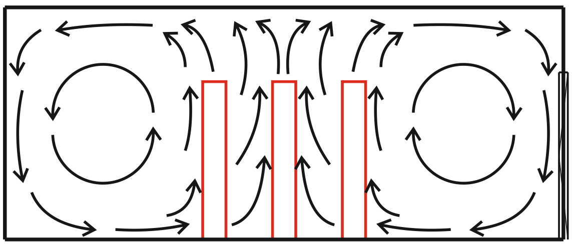

Figure 5.10. Air movement with heat loads centered (position 1).

With heat loads in the middle of the room, the thermal plume from the heat sources made the smoke rise until it deflected off of the ceiling, moving towards all four walls before falling towards the floor. This flow solution seemed stable. Afterwards the the manikins were put in one end of the room as shown in figure 5.11.

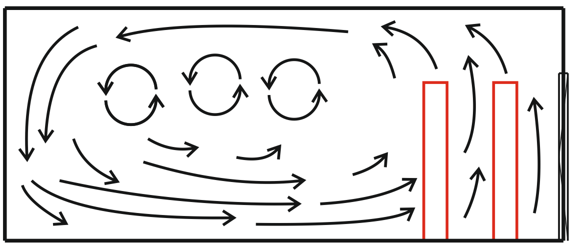

Figure 5.11. Air movement with heat loads in one end (position 2).

This solution was more stable than with maniniks in the center of the room, the smoke was supplied close to the manikins, rose to the ceiling and moved towards the opposite wall before falling to the floor. Heat load distribution was also the one showing the most consistent results when creating the design charts.

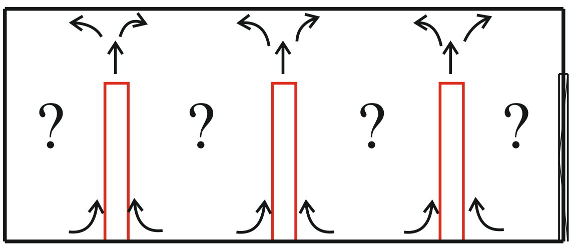

Figure 5.12. Air movement with heat loads evenly distributed (position 3).

Both heat load positions 1 and 2 show fairly consistent tendencies, but with position 3 it was not possible to conclude anything specific. The arrows shown in figure 5.12 are the areas where it was easy to see the direction of the flow, in the other areas the direction was either unclear or not consistent. It seems that in many of the regions where the flow could possibly flow downward, there was still a heat source in the vicinity which could deflect the flow.

5.4.2 Velocity depiction

Velocity depictions are made to show the velocities in various points in the test room. The presented velocities were, in each case, measured with the same flow rate so only positions of measurement equipment and manikins changed.

2.5 m modular ceiling

With a room height of 2.5 m, the lowest velocities compared to the other room height were observed. Figure 5.13 shows a velocity depiction for the three different heat load distributions. For comparison equal flow rates of 0.179 m^3/s are shown.

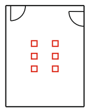

		Velocity [m/s]		
Corner pole	1.7 m			0,03
	1.1 m			0,04
	0.1 m			0,06
		A	B	C
4	1.7 m	0,10	0,10	0,06
	1.1 m	0,09	0,09	0,08
	0.1 m	0,04	0,08	0,06
3	1.7 m	0,09	0,09	0,05
	1.1 m	0,04	0,04	0,05
	0.1 m	0,10	0,08	0,11
2	1.7 m	0,07	0,07	0,04
	1.1 m	0,04	0,04	0,04
	0.1 m	0,07	0,07	0,12
1	1.7 m	0,10	0,06	0,05
	1.1 m	0,07	0,05	0,03
	0.1 m	0,05	0,05	0,06

(a) Case 1c

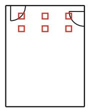

		Velocity [m/s]		
Corner pole	1.7 m			0,05
	1.1 m			0,09
	0.1 m			0,03
		A	B	C
4	1.7 m	0,09	0,06	0,07
	1.1 m	0,04	0,03	0,05
	0.1 m	0,11	0,18	0,16
3	1.7 m	0,09	0,06	0,08
	1.1 m	0,03	0,03	0,03
	0.1 m	0,14	0,18	0,17
2	1.7 m	0,12	0,09	0,09
	1.1 m	0,04	0,07	0,05
	0.1 m	0,12	0,13	0,13
1	1.7 m	0,09	0,08	0,09
	1.1 m	0,08	0,08	0,10
	0.1 m	0,03	0,06	0,05

(b) Case 2c

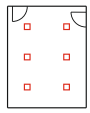

		Velocity [m/s]		
Corner pole	1.7 m			0,07
	1.1 m			0,09
	0.1 m			0,03
		A	B	C
4	1.7 m	0,07	0,06	0,07
	1.1 m	0,05	0,04	0,07
	0.1 m	0,05	0,09	0,07
3	1.7 m	0,10	0,05	0,06
	1.1 m	0,06	0,06	0,04
	0.1 m	0,06	0,04	0,04
2	1.7 m	0,08	0,10	0,04
	1.1 m	0,05	0,05	0,05
	0.1 m	0,07	0,06	0,05
1	1.7 m	0,08	0,07	0,08
	1.1 m	0,08	0,07	0,09
	0.1 m	0,07	0,04	0,05

(c) Case 3c

Figure 5.13. Velocity distribution in the room with a ceiling height of 2.5 m.

In case 1c shown in figure 5.13(a) the velocities did not vary much from one position to another. Relatively high velocities occurred in the sides of the room due to the downward flow close to the walls, which was created by the buoyant flow from the manikins positioned in the middle of the room. Smoke measurements showed this tendency, shown in figure 5.10 on the previous page.

In case 2c, figure 5.13(b), the manikins were positioned in one end of the room and as expected, the highest velocities occurred close to the floor in some distance from the opposite wall as the where the manikins were positioned. The large plume from the manikins rose and floated along the ceiling, being cooled by the colder supply, until it went downward at the opposite wall of the room, from where it increased in velocity onto the floor.

The last heat load distribution, case 3c, had the manikins evenly distributed in the room. Figure 5.13(c) shows very similar velocities in the entire room which indicates a very good mixing of the air. What is interesting is that the highest velocities occurred in a height of 1.7 m which could indicate that the air rose along the walls and dropped in the middle of the room. The velocities were in general very similar, and low compared to the other cases.

4.1 m modular ceiling

Figure 5.13 on the facing page shows the velocity distribution for the three cases with room height of 4.1 m. For comparison equal flow rates of 0.193 m^3/s are shown.

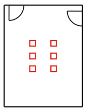

Velocity [m/s]				
Corner pole		1.7 m		0,11
		1.1 m		0,07
		0.1 m		0,07
		A	B	C
4	1.7 m	0,12	0,14	0,06
	1.1 m	0,12	0,13	0,07
	0.1 m	0,13	0,14	0,10
3	1.7 m	0,07	0,08	0,05
	1.1 m	0,08	0,07	0,06
	0.1 m	0,17	0,11	0,12
2	1.7 m	0,05	0,07	0,08
	1.1 m	0,10	0,06	0,09
	0.1 m	0,14	0,09	0,10
1	1.7 m	0,11	0,06	0,11
	1.1 m	0,08	0,08	0,05
	0.1 m	0,07	0,07	0,08

(a) Case 4c

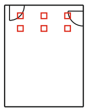

Velocity [m/s]				
Corner pole		1.7 m		0,11
		1.1 m		0,13
		0.1 m		0,03
		A	B	C
4	1.7 m	0,05	0,08	0,06
	1.1 m	0,07	0,12	0,05
	0.1 m	0,23	0,23	0,21
3	1.7 m	0,04	0,06	0,05
	1.1 m	0,07	0,11	0,07
	0.1 m	0,23	0,22	0,20
2	1.7 m	0,07	0,07	0,10
	1.1 m	0,11	0,09	0,13
	0.1 m	0,18	0,15	0,13
1	1.7 m	0,15	0,15	0,14
	1.1 m	0,11	0,09	0,09
	0.1 m	0,09	0,08	0,06

(b) Case 5c

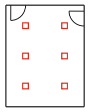

Velocity [m/s]				
Corner pole		1.7 m		0,12
		1.1 m		0,09
		0.1 m		0,04
		A	B	C
4	1.7 m	0,10	0,08	0,06
	1.1 m	0,11	0,09	0,05
	0.1 m	0,16	0,16	0,13
3	1.7 m	0,08	0,09	0,05
	1.1 m	0,09	0,10	0,05
	0.1 m	0,19	0,17	0,15
2	1.7 m	0,07	0,08	0,09
	1.1 m	0,12	0,09	0,10
	0.1 m	0,15	0,13	0,10
1	1.7 m	0,11	0,09	0,13
	1.1 m	0,09	0,07	0,10
	0.1 m	0,15	0,09	0,07

(c) Case 6c

Figure 5.14. Velocity distribution in the room with a ceiling height of 4.1 m

Compared to a room height of 2.5 m, the magnitude of the velocities was larger with a room height of 4.1 m. Once again, with manikins in the center of the room, figure 5.14(a), the highest measured velocities occurred in the side of the room.

In case 5c, figure 5.14(b) the tendency was the same as when having a room height of 2.5 m. Velocities were low close to the wall opposite the manikins, but increased towards the middle of the room. All measurements with this heat load distribution showed very consistent results.

Case 6c on figure 5.14(c) is quite different than case 3c. The velocities close to the floor were way higher than in the other parts of the the room. Case 3c (figure 5.14(b)) showed signs of good mixing in the room, but this was not the situation in case 6c. This could be due to the fact that two different flow solutions were present in the two cases. This is investigated further in section 5.4.3 on the next page where the flow over time is analysed.

4.4 m diffuse acoustic ceiling

Figure 5.13 on the facing page shows the velocity distribution for the three cases with room height of 4.4 m. For comparison equal flow rates of 0.201 m^3/s are shown.

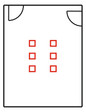		Velocity [m/s]		
		Corner pole	1.7 m	0,22
			1.1 m	0,20
			0.1 m	0,08
		A	B	C
4	1.7 m	0,13	0,15	0,07
	1.1 m	0,13	0,12	0,10
	0.1 m	0,11	0,12	0,11
3	1.7 m	0,08	0,08	0,05
	1.1 m	0,09	0,08	0,05
	0.1 m	0,15	0,12	0,16
2	1.7 m	0,08	0,08	0,08
	1.1 m	0,13	0,07	0,10
	0.1 m	0,12	0,08	0,11
1	1.7 m	0,12	0,09	0,09
	1.1 m	0,10	0,09	0,06
	0.1 m	0,08	0,07	0,08

(a) Case 7c

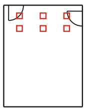		Velocity [m/s]		
		Corner pole	1.7 m	0,12
			1.1 m	0,14
			0.1 m	0,04
		A	B	C
4	1.7 m	0,06	0,09	0,06
	1.1 m	0,08	0,13	0,06
	0.1 m	0,23	0,25	0,23
3	1.7 m	0,05	0,08	0,04
	1.1 m	0,07	0,12	0,06
	0.1 m	0,23	0,21	0,21
2	1.7 m	0,09	0,08	0,07
	1.1 m	0,13	0,12	0,09
	0.1 m	0,17	0,13	0,14
1	1.7 m	0,20	0,12	0,15
	1.1 m	0,17	0,10	0,10
	0.1 m	0,10	0,09	0,09

(b) Case 8c

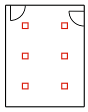		Velocity [m/s]		
		Corner pole	1.7 m	0,13
			1.1 m	0,12
			0.1 m	0,05
		A	B	C
4	1.7 m	0,09	0,09	0,07
	1.1 m	0,11	0,10	0,07
	0.1 m	0,19	0,19	0,13
3	1.7 m	0,07	0,10	0,05
	1.1 m	0,09	0,11	0,06
	0.1 m	0,20	0,19	0,14
2	1.7 m	0,09	0,11	0,09
	1.1 m	0,10	0,11	0,09
	0.1 m	0,19	0,14	0,14
1	1.7 m	0,14	0,12	0,11
	1.1 m	0,13	0,10	0,09
	0.1 m	0,11	0,09	0,10

(c) Case 9c

Figure 5.15. Velocity distribution in the room with a ceiling height of 4.4 m

Case 7c on figure 5.15(a) showed same trend as with other room heights, but also very high velocities in the corners. Case 8c on figure 5.15(b) also shows the same as in the other situations, that the velocities increased towards the middle of the room. Case 9c on figure 5.15(c) showed similar tendencies as case 6c, where high velocities occurred close to the floor and not in a height of 1.7 m as in case 3c.

5.4.3 Air flow stability

All measurements were performed in steady state, meaning conditions in the test room did not change over time. Chodor and Taradajko [2013] also performed measurements in steady state, however especially with evenly distributed heat loads, experiments showed that the velocities were unstable over time. In this section, the velocities over time are presented and analysed to determine whether the flow was stable or unstable/unsteady. Unsteady flow could indicate that the flow in the room had two or more solutions. The presented measurements of velocities are shown for the anemometer measuring the highest velocities for each heat load distribution. This study is more an analysis of the resulting flow situations when varying heat load distributions than a study of room height. Room height have shown to not have a great effect on the flow pattern as shown in the previous section. In this section a few representative situations are shown.

It is chosen to investigate the stability of the airflow with a ceiling height of 4.4 m. Again the flow rate to the room is equal in the presented cases, that being 0.201 m^3/s. Each measuring period had a duration of 15 min (900 s) and velocities were logged every 0.1 s.

Heat loads centered (case 7c)

First up is case 7c which had manikins centered in the middle of the room. The velocity distribution is shown in figure 5.15(a) and the highest velocities were measured in measurement position 3C (see figure 4.7 on page 28) close to wall 2 in a height of 0.1 m. The velocity distribution along with the frequency of velocities for this case is shown in figure 5.16 on the facing page.

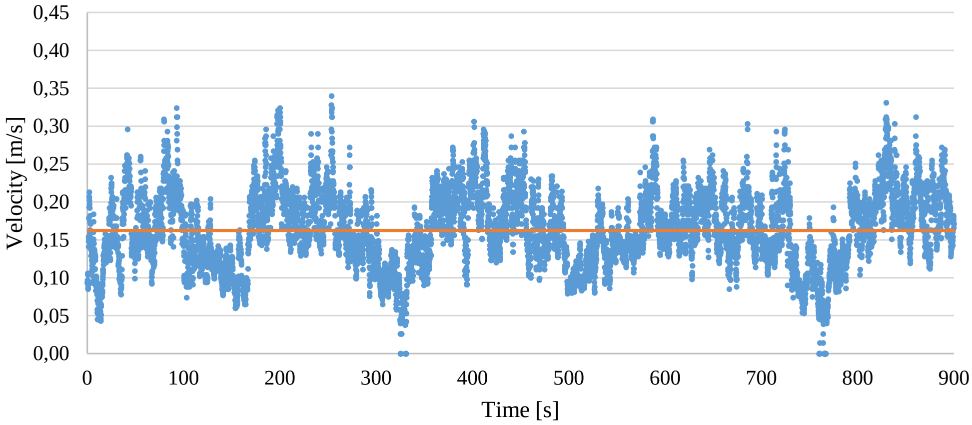

(a) Case 7c velocity distribution.

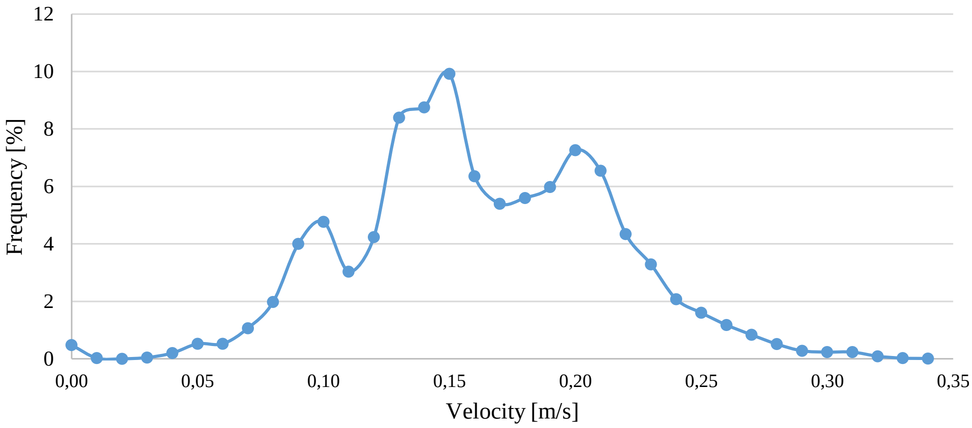

(b) Case 7c velocity occurrence.

Figure 5.16. Velocities over time and how often specific magnitudes of velocities occurred, case 7c.

The velocity distribution on figure 5.16(a) is fairly centered around the average of 0.16 m/s but has some interesting drops and rises along the measurement period. The velocity reached four low points during the 900 seconds, namely at approximately 150, 300, 500 and 750 seconds. This indicates that the flow was not as steady as expected. The change can be caused by the air flowing towards walls 1 and 3 in some periods and walls 2 and 4 in other.
Figure 5.16(b) shows the occurrence frequency of velocities for case 7c. Velocities were rounded off to closest value with two digits. If the flow was very stable, it would show a distribution associated with a normal distribution. The distribution shows that the velocity occurring most frequent is very close to the average velocity but also that a higher and lower velocity had high occurrences.

Heat loads in one end (case 8c)

For heat loads positioned in one end of the room, the velocity over time in the point measuring the highest velocity is shown in figure 5.17 on the next page. Highest velocities were measured in measurement position 4B in a height of 0.1 m.

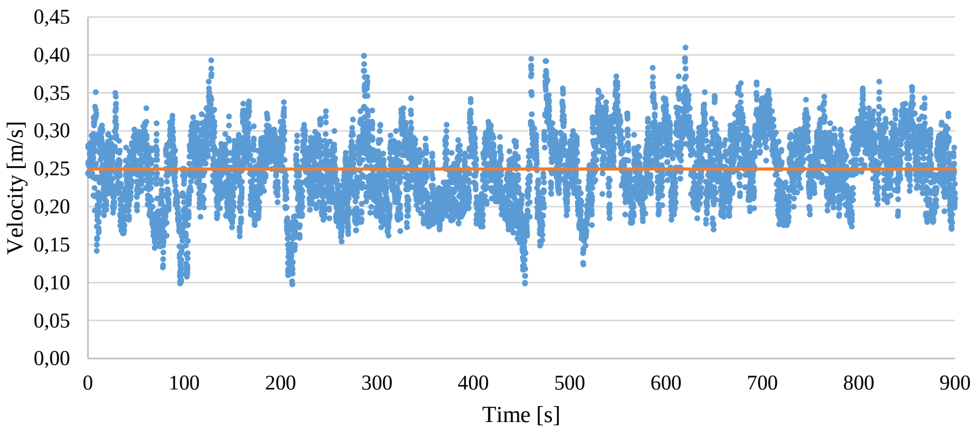

(a) Case 8c velocity distribution.

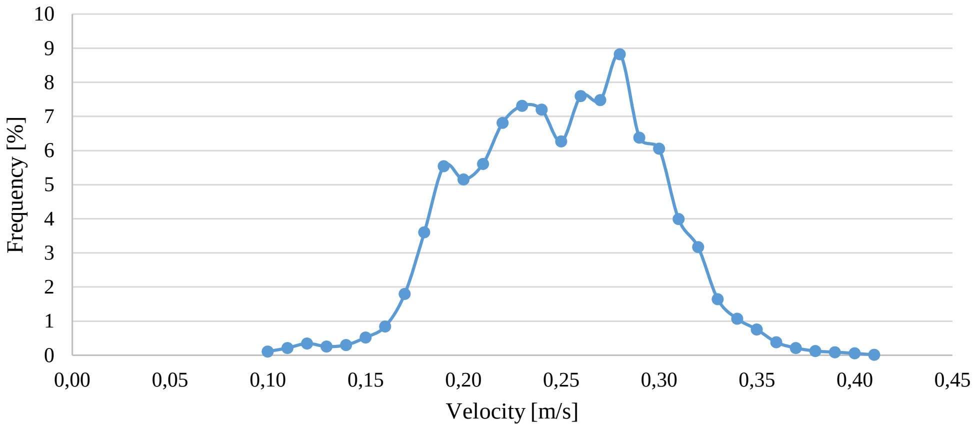

(b) Case 8c velocity occurrence.

Figure 5.17. Velocities over time and how often specific magnitudes of velocities occurred, case 8c.

Having heat loads in one end, the logged values were all fairly close to the average value. In this case the flow was very stable and the fluctuations in figure 5.17(a) is a sign of turbulence rather than instability. The graph in figure 5.17(b) can be associated with a normal distribution, which is also expected in case of stable flow.

Heat loads evenly distributed (case 9c)

With heat loads evenly distributed the air flow pattern was more difficult to predict while the two other heat load positions seemed more obvious. The velocities measured in measurement point 3A in a height of 0.1 m are depicted in figure 5.18 on the facing page.

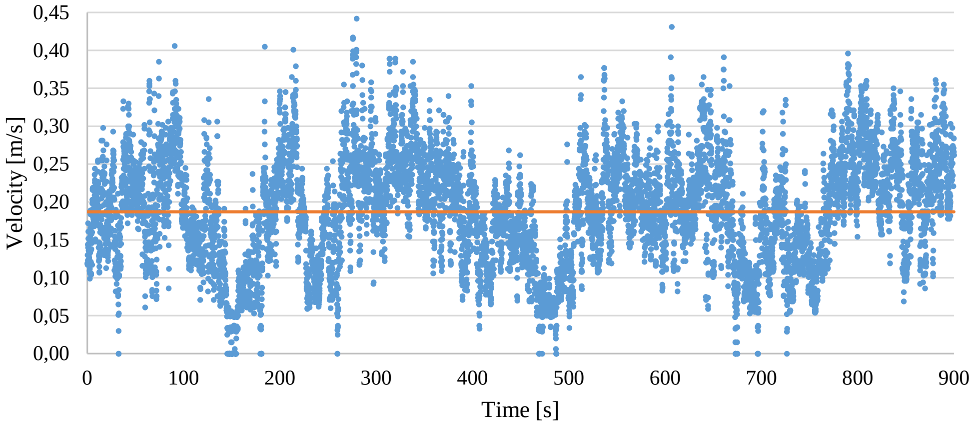

(a) Case 9c velocity distribution.

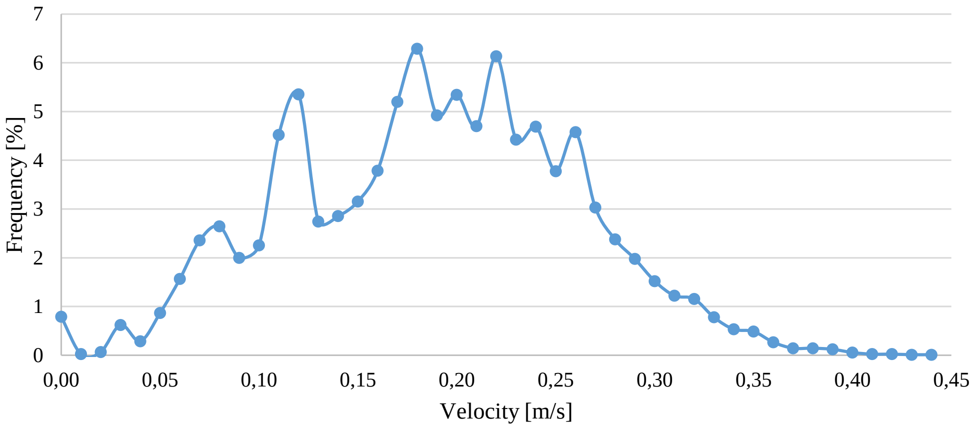

(b) Case 9c velocity occurrence.

Figure 5.18. Velocities over time and how often specific magnitudes of velocities occurred, case 9c.

Figure 5.18(a) shows some very intense fluctuations in the measured velocities. At first sight the velocity pattern looks very chaotic but looking closer the velocities seemed to be periodically high and low. The duration of each high period was approximately 150 seconds after which the velocities dropped for a while before increasing again. Intervals with high velocities occurred in approximately 0-150 s, 250-400 s, 500-680 s and 780-900 s. In these periods the average velocity was fairly close to 0.25 m/s, in other words somewhat higher than the average measured over 900 seconds of 0.20 m/s.
The frequency of each velocity magnitude is shown in figure 5.18(b) and shows that a variety of different velocities occurred often during the 900 seconds. This indicates that the velocities never found a stable condition but changes frequently. Velocities in a range from 0.12 m/s to 0.26 m/s occurred with more or less equal frequency! Since the calculated cooling capacities of the system were based on the average velocity, these results could indicate that when having evenly distributed heat loads, the system does not perform as well as earlier assumed.

5.5 Temperature distribution

One of the main advantages with diffuse ceiling ventilation is that the air in the room typically becomes very well mixed, and that temperature differences in the occupied zone are almost non-existing. To verify if this is the case, this section contains a collection of obtained temperatures from the occupied zone, namely the temperature distribution in the room and vertical temperature differences. Asymmetric radiant temperature is also measured and results can be found on Appendix cd, but they are not shown in the report because the asymmetric temperature are very low.

Temperature depiction

In the previous section the velocity distribution was analysed for the three different ceiling heights. Many similarities were observed, and the velocity distribution was in many cases unchanged when changing ceiling height, though the magnitude of the velocities changed significantly. The main differences in velocity distribution were observed when changing the heat loads. The same tendency applied for the temperature distribution, changing ceiling did not change the resulting temperatures much. Therefore the temperature distribution in the room is only shown for cases 7, 8 and 9 - the cases with a ceiling height of 4.4 m - shown in figure 5.19. The other cases can be found on Appendix CD.

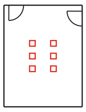		Temperature [°C]		
		Corner pole	1.7 m	19,56
			1.1 m	19,60
			0.1 m	19,79
		A	B	C
4	1.7 m	19,86	19,88	19,84
	1.1 m	19,92	20,17	19,87
	0.1 m	19,95	20,15	19,88
3	1.7 m	19,82	19,88	19,83
	1.1 m	19,88	20,06	19,88
	0.1 m	19,86	19,98	19,86
2	1.7 m	19,83	19,91	19,80
	1.1 m	19,85	19,90	19,82
	0.1 m	19,83	19,88	19,91
1	1.7 m	19,80	19,91	19,85
	1.1 m	19,90	19,91	19,90
	0.1 m	19,87	19,83	19,80

(a) Case 7c

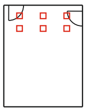		Temperature [°C]		
		Corner pole	1.7 m	20,19
			1.1 m	20,17
			0.1 m	20,35
		A	B	C
4	1.7 m	20,16	20,18	20,21
	1.1 m	20,20	20,22	20,25
	0.1 m	20,12	20,01	20,10
3	1.7 m	20,14	20,14	20,14
	1.1 m	20,15	20,14	20,15
	0.1 m	20,04	20,00	20,06
2	1.7 m	20,02	20,07	20,01
	1.1 m	20,01	20,01	20,02
	0.1 m	19,96	19,95	20,05
1	1.7 m	19,80	20,02	19,86
	1.1 m	19,93	20,04	19,97
	0.1 m	19,93	19,93	19,93

(b) Case 8c

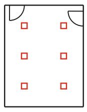		Temperature [°C]		
		Corner pole	1.7 m	19,83
			1.1 m	19,88
			0.1 m	20,02
		A	B	C
4	1.7 m	19,94	19,81	19,95
	1.1 m	20,10	19,95	20,01
	0.1 m	19,96	19,80	19,92
3	1.7 m	19,92	19,81	19,92
	1.1 m	19,96	19,95	19,95
	0.1 m	19,89	19,79	19,95
2	1.7 m	19,90	19,80	20,04
	1.1 m	20,09	19,86	20,05
	0.1 m	19,87	19,79	20,02
1	1.7 m	19,74	19,79	19,79
	1.1 m	19,87	19,92	19,92
	0.1 m	19,85	19,80	19,84

(c) Case 9c

Figure 5.19. Temperature distribution in the room with a ceiling height of 4.4 m.

Figure 5.19(a) shows a very uniform temperature distribution, other than in positions 3B and especially 4B which were also in the vicinity of the manikins and therefore not surprisingly slightly effected by their heat release.
When the manikins were positioned in one end of the room (figure 5.19(b)), the upward flow from plumes rose and moved along the ceiling to the other end of the room - simultaneously being cooled down - before dropping at the other wall and increase in temperature towards the middle of the room.
Figure 5.19(c) shows something unexpected. So far it has been unclear how the airflow with evenly distributed heat sources was, but the temperature distribution can help us identifying at least one solution. The cold regions in the middle of the room can indicate that the air rose close to the walls and dropped in the middle of the room. If another flow solution would be present it could be the other way around, that the cold air went down

along the walls and warmer air rose in the middle of the room, but no measurements can validate this theory.

5.5.1 Other indoor climate parameters

As mentioned in section 3 on page 19, other indoor climate parameters are also important to consider. The results for draught, vertical temperature gradients and radiant temperature asymmetry are shown in the following.

Draught rate

Draught rate was explained in chapter 3 and the draught ratings are explained shortly in this section. The formula for measuring draught rate is only applicable if the air temperature is in the interval from 20 to 26 °C. Some measurements were conducted at low temperatures in this interval and some at higher temperatures, not really trying to obtain a good comfort temperature but rather similar temperatures as in the laboratory. Therefore the draught rate evaluation is modified slightly, and is evaluated from a constant temperature of 23 °C. This gives an overview of the draught rate at a normal indoor temperature, and shows the correlation between local air velocity and turbulence intensity.

In many of the experiments, velocities above 0.15 m/s were observed. However, a high average air velocity often corresponds to a low level of turbulence. Only in cases with the diffuse acoustic ceiling and manikins in one end of the room, draught ratings above 20 % were experienced. A figure in which the draught rate for the three heat load distributions are compared is shown in figure 5.20. Draught ratings above 20 % only occurred at the highest tested flow rate of 0.296 m^3/s.

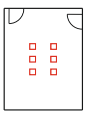

		Draught rate [%]		
Corner pole	1.7 m			17
	1.1 m			19
	0.1 m			4
		A	B	C
4	1.7 m	8	14	4
	1.1 m	9	9	7
	0.1 m	8	9	9
3	1.7 m	6	7	2
	1.1 m	7	7	3
	0.1 m	13	10	12
2	1.7 m	6	6	5
	1.1 m	9	5	6
	0.1 m	12	5	8
1	1.7 m	14	6	10
	1.1 m	11	7	3
	0.1 m	5	5	5

(a) Case 7d

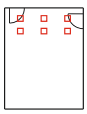

		Draught rate [%]		
Corner pole	1.7 m			10
	1.1 m			11
	0.1 m			8
		A	B	C
4	1.7 m	3	7	1
	1.1 m	4	10	3
	0.1 m	21	21	20
3	1.7 m	2	5	8
	1.1 m	4	10	2
	0.1 m	21	20	17
2	1.7 m	2	8	8
	1.1 m	8	13	12
	0.1 m	16	10	10
1	1.7 m	18	10	11
	1.1 m	16	7	5
	0.1 m	8	8	7

(b) Case 8d

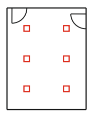

		Draught rate [%]		
Corner pole	1.7 m			16
	1.1 m			15
	0.1 m			2
		A	B	C
4	1.7 m	7	6	4
	1.1 m	9	5	5
	0.1 m	18	12	11
3	1.7 m	3	6	1
	1.1 m	6	8	3
	0.1 m	18	17	11
2	1.7 m	7	9	8
	1.1 m	12	10	10
	0.1 m	14	10	8
1	1.7 m	17	10	6
	1.1 m	16	8	5
	0.1 m	9	9	6

(c) Case 9d

Figure 5.20. Draught rate in the different heat load positions with a room height of 4.4 m.

Often the draught rate is high due to high velocities which is what happened in case 8d, where the turbulence is low. In case 9d the velocities were actually significantly lower, but the draught rate is only slightly lower. This is because the local turbulence intensity is much higher than in case 8d, giving a high draught rating even though velocities were not alarmingly high. In all other measured situations the draught rate was lower than 20 % and in most cases much lower. The velocities, turbulence intensity and draught rating for all cases can be found on the Appendix CD.

Vertical temperature gradient

Another way of evaluating the thermal climate in a room is by measuring the vertical temperature gradient. First of all it should be emphasized that the temperature gradient does not change much from any experiment to another. In the report situations for all three room heights and flow rates of 0.179 m^3/s (2.5 m), 0.193 m^3/s (4.1 m) and 0.201 m^3/s (4.4 m) are shown. Temperature gradients for the three ceiling heights are shown in figure 5.21.

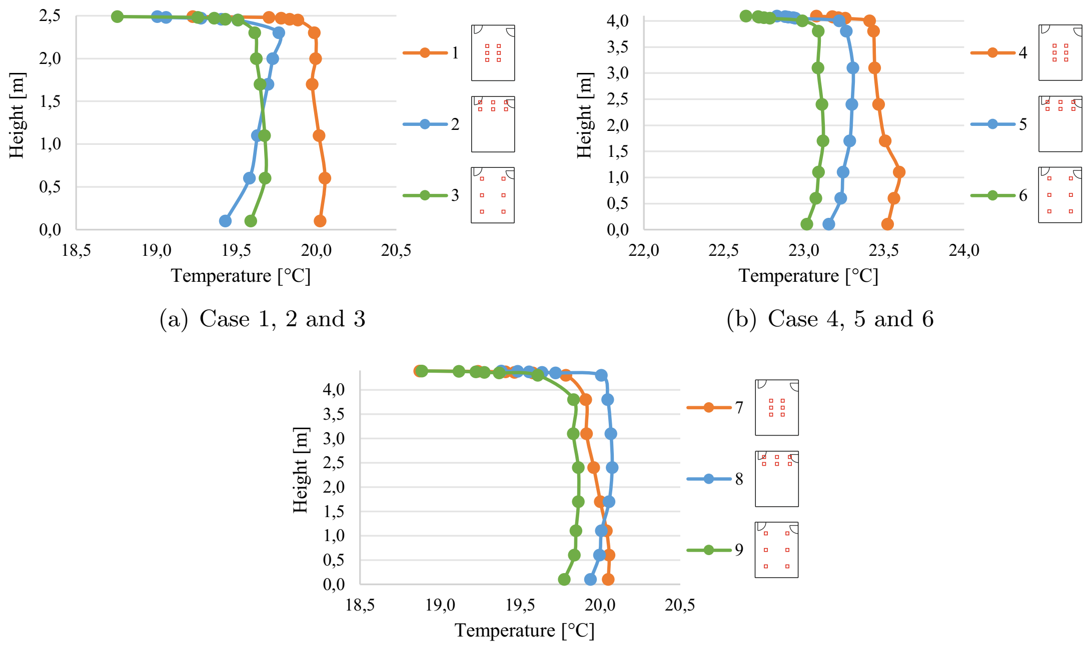

(a) Case 1, 2 and 3

(b) Case 4, 5 and 6

(c) Case 7, 8 and 9

Figure 5.21. Temperature gradients for the three different room heights.

The temperature gradients were very similar, naturally cases 1, 4 and 7 were a little higher than the others (especially close to the floor) since the manikins were positioned fairly close to the measuring points. In all three cases the temperature dropped close to the ceiling, where cold air was supplied. The drop was quite small and could suggest that the supply air in all three cases mixed very quickly with the air in the room. What is also interesting is that the vertical temperature gradient was very low in all situations (<0.5 °C) [DS/CEN/CR 1752, 2001].

To compare the vertical temperature gradients to each other in the different cases, both the room height and the temperature is made dimensionless based on the equations 5.3 on the facing page and 5.4 on the next page. The dimensionless temperature gradients are shown in figure 5.22 on the facing page. [Nielsen, 1999]

$$t^* = \frac{t_l - t_s}{t_e - t_s} \tag{5.3}$$

$$h^* = \frac{h}{H} \tag{5.4}$$

Where:

t^*	Dimensionless temperature [-]
t_l	Local temperature [°C]
t_s	Supply temperature [°C]
t_e	Extract temperature [°C]
h^*	Dimensionless dimensionless height [-]
h	Local height [m]
H	Total room height [m]

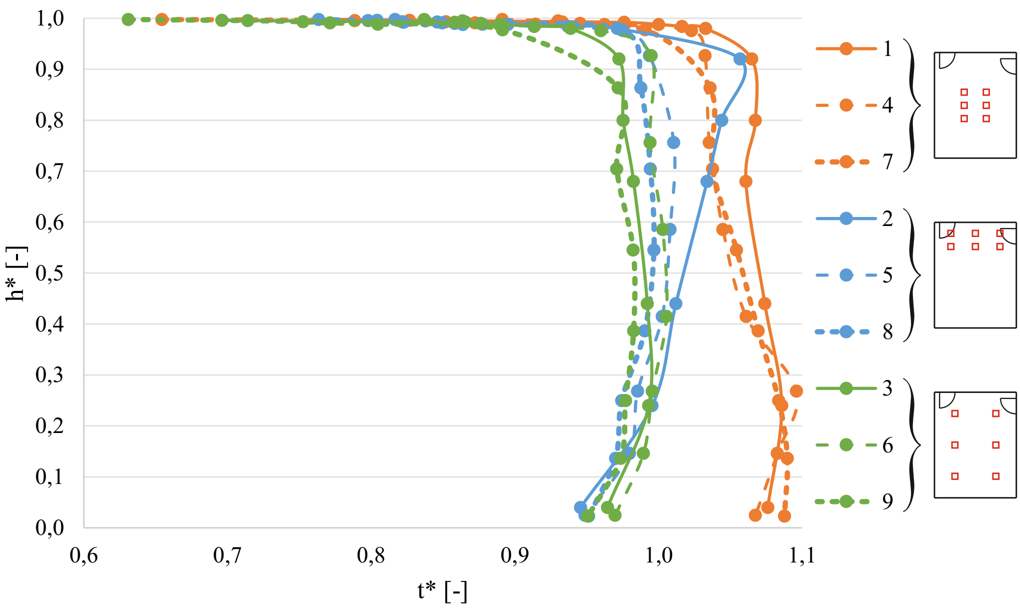

Figure 5.22. Comparison of vertical temperature gradients with respect to ceiling height and heat load distribution.

The figure shows that the individual heat load position had an effect on the vertical temperature gradient, and that the room height and/or ceiling type had very little influence.

Radiant temperature asymmetry

The results showed almost no radiant temperature asymmetry. Maximum observed vertical temperature asymmetry was 2.62 K, which is clearly within the limits of 14 K. Horisontal temperature asymmetry was limited to 0.61 K which is also within the limits of 5 K. [DS/EN ISO 7730, 2006]

CFD predictions 6

This chapter contains a set of CFD predictions made in order to support the experimental results. CFD models which can be compared with measurements are created in the program FloVENT. Furthermore CFD predictions can help visualise flow patterns to help give further insight in the processes taking place in the test chamber. First computational fluid dynamics in general is introduced.

6.1 Computational Fluid Dynamics

Fluid flow and heat transfer are governed by conservation laws that can be expressed in a partial differential form. The conservation laws are based on the principles of conservation of mass, momentum and energy and stated in the following:

- The mass of a fluid is conserved (continuity equation)
- The rate of change of momentum equals the sum of forces on a fluid particle (Newton's second law, Navier-Stokes equations)
- The rate of change of energy is equal to the sum of the rate of heat addition to and the rate of work done on a fluid particle (first law of fluid dynamics, energy equation)

The conservation equations are converted to a finite volume (FVM) form and the variables temperature, pressure and velocity are then calculated for each control volume (CV) specified in the solution domain.

Slightly simplified, the three above statements are regarded as the conservative form of the governing equations of fluid flow and can be expressed as the continuity equation, three-dimensional momentum equation and energy equation. A general transport equation to solve a general variable ϕ can be defined as in equation 6.1. [Nielsen et al., 2007]

$$\underbrace{\frac{\partial (\rho\phi)}{\partial t}}_{\text{Transient}} + \underbrace{\nabla (\rho\phi u)}_{\text{Convective}} = \underbrace{\nabla (\Gamma \nabla \phi)}_{\text{Diffusive}} + \underbrace{S_\phi}_{\text{Source term}} \tag{6.1}$$

This equation represents the conservation of ϕ. The single terms in the equation can be explained as:

$\frac{\partial(\rho\phi)}{\partial t}$	Variation of ϕ over time, where ρ is the density of the fluid
$\nabla(\rho\phi u)$	The net quantity of ϕ brought by the flow with velocity (u, v, w) through the surface of a control volume (convection)
$\nabla(\Gamma\nabla\phi)$	Net flux of ϕ through the surface of a control volume, where Γ represents the diffusion coefficient of ϕ (diffusion)
S_ϕ	Source term which represents the creation of ϕ per unit of volume and time
ρ	Density of air [kg/m^3]
∇	Divergence operator, in three dimensions $\frac{\partial}{\partial x}$, $\frac{\partial}{\partial y}$ and $\frac{\partial}{\partial z}$
Γ	Diffusion coefficient [m^2/s]

Relevant entries for ϕ are shown in table 6.1.

	ϕ	Γ	S_ϕ
Continuity	1	0	0
x-momentum	u	μ	$-\frac{\partial p}{\partial x} + \rho_x g$
y-momentum	v	μ	$-\frac{\partial p}{\partial y} + \rho_y g$
z-momentum	w	μ	$-\frac{\partial p}{\partial z} + \rho_z g$

Table 6.1. Dependent variables in the general transport equation.

How this theory is applied in FloVENT is explained in Appendix F.

6.2 Reference model based on case 2a

A reference model is set up in FloVENT with the purpose to be the basis of following CFD predictions. The model is set up as close to experiment conditions as possible and compared to the experimental results for validation. Assumptions and inputs to the reference model are explained in the following.

The model is set up as close to the experimental conditions that occurred in case 2a. A picture of the reference model is shown in figure 6.1 on the next page.

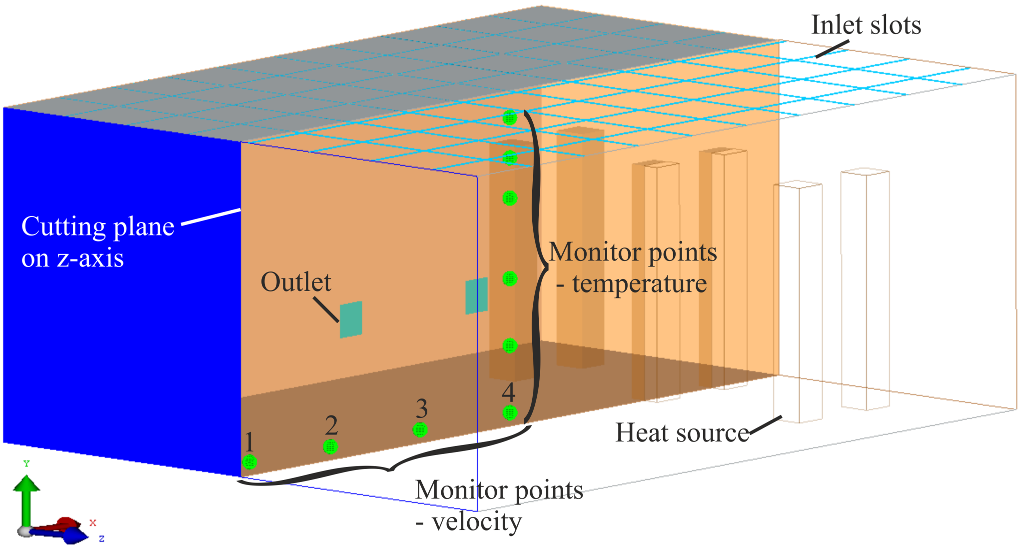

Figure 6.1. Reference model showing room, heat sources and air distribution geometry. Furthermore monitor points used for grid independence study and validation with experimental results are shown.

6.2.1 Geometry

The model is built so the geometry of the room is as similar to the real test room as possible. The dimensions of the room is 6.0 x 4.65 x 2.5 m. Construction of surfaces and their roughness are made as shown in table 6.2. In the model there is no conductive heat transfer towards the ambient.

Surface	Material	Roughness [m]
Wall 1 (door)	Fibreboard	0.013
Wall 2 (gypsum)	Plasterboard	0.013
Wall 3 (glass)	Mainly glass	0.011
Wall 4 (outlet)	Fibreboard	0.013
Floor	Fibreboard	0.013
Ceiling	Insulation	0.015

Table 6.2. Roughness of surfaces of test room estimated from The Engineering Toolbox [2014]

6.2.2 Inlet slots

The real ceiling used with a room height of 2.5 m consisted of quadratic stone wool elements resting on reversed T-profiles. Smoke experiments showed that the air mainly passed between the ceiling elements and aluminium profiles. Visualisation of both construction of ceiling and smoke experiment is shown in figure 5.9 on page 46. In the CFD model, the supply geometry is therefore created as the reversed T-profiles in a width of 20 mm, see "Inlet slots" in figure 6.1.

6.2.3 Heat sources

The actual manikins have different shapes as shown in figure 4.12 on page 31. For simplification in the CFD model, the heat loads all have the similar geometries, all being 1.75 x 0.25 x 0.25 m equaling a total surface area of 1.875 m^2 per manikin.

In the experiments, manikins were supplied 77 W corresponding to the free heat release from a person at sedentary (office) activity. Since radiation is disabled in the CFD model the radiative part of the heat release is neglected. Hyldgård et al. [1997] suggests the ratio between convective and radiative heat release varies significantly at different air velocities. Following heat release can be expected, see table 6.3.

Air velocity [m/s]	Heat release (convection) [W]	Heat release (radiation) [W]
< 0.1	36	38
< 0.3	47	29

Table 6.3. Heat release due to convection and radiation at different temperatures. This heat release corresponds to sedentary activity. [Hyldgård et al., 1997]

Since the highest velocities measured in the test room did not exceed 0.2 m/s, interpolating between 36 and 47 W yields 41.5 W as convective heat release. This power is applied to each heat source in the CFD reference model.

6.2.4 Boundary conditions

For comparison with experimental case same air flow conditions and surface temperatures are applied.

Inlet slots are created as "Fixed flow - inlet" and the total flow rate of 0.055 m^3/s, corresponding to an air change rate of 2.84 h^{-1} is divided evenly over the total number of inlet slots which are of same size. Inlet temperature is set to 16.33 °C.

Outlet ducts are created as "Fans" meaning they have a specified flow rate but also the ability to increase or decrease to some extend dependent on the pressure. This way the outlets take into consideration that the density of the air changes in the room, and a mass balance can be sustained. Outlets are simplified and have a rectangular form in the CFD model, while they in reality are circular.

Since radiation is disabled, the temperature of the internal surfaces of the room must be prescribed. They were measured in during experiments with two thin thermocouples on each surface and are shown in table 6.4 on the next page.

Surface	Temperature [°C]
Wall 1 (door)	21.02
Wall 2 (gypsum)	19.98
Wall 3 (glass)	20.24
Wall 4 (outlet)	20.31
Floor	20.67
Ceiling	19.62

Table 6.4. Surface temperatures of test room.

As mentioned the CFD simulations are all carried out in steady-state conditions.

6.2.5 Grid independence

The calculated velocities and temperatures should not be significantly influenced by the density of the mesh in the solution domain. To ensure that, and to save computational time for future CFD predictions, a small study is performed to test how dense the grid needs to be before the model is independent on the number of grid cells. The study is evaluated on basis of velocities in the room, namely the velocity in x-direction in four monitor points, which can be seen in figure 6.1 on page 61. The resulting velocities are shown in table 6.5.

Grid independence	Cells [#]	xvel, mp1 [m/s]	xvel, mp2 [m/s]	xvel, mp3 [m/s]	xvel, mp4 [m/s]
Mesh 1	19456	0.093	0.158	0.165	0.160
Mesh 2	35200	0.090	0.165	0.172	0.164
Mesh 3	64119	0.089	0.166	0.173	0.165
Mesh 4	126380	0.063	0.157	0.168	0.162
Mesh 5	247296	0.043	0.136	0.149	0.137
Mesh 6	617400	0.024	0.148	0.160	0.146
Mesh 7	1289472	0.024	0.152	0.162	0.146

Table 6.5. Velocities in x-direction for the four monitor points used for testing grid independence.

The velocities do not change significantly after mesh 6 with 617400 cells for which reason this mesh density is chosen for the reference model. A graph showing the resulting velocities is shown in figure 6.2 on the following page.

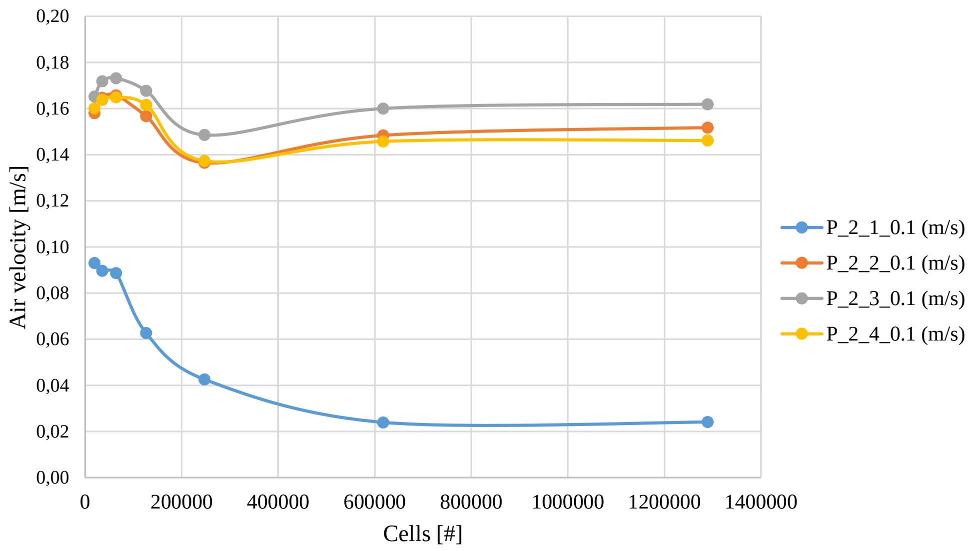

Figure 6.2. Graphs showing how velocities in four different points develop when making grid finer.

Figures of the velocity and temperature distribution in each grid test are shown in Appendix G. The cutting plane on z-axis shown in figure 6.1 on page 61 go through the middle of the room and thereby also straight through the middle of the two heat sources in the middle. If nothing else is specified, this cutting plane is used for visualisation.

6.2.6 Validation of reference model

Next, results from the reference model are compared to measured values. Both temperature and velocities are compared from the points shown in figure 6.1 on page 61.

When performing measurements, the velocity was measured in the four points, 1B, 2B, 3B and 4B (see figure 4.7 on page 28) and the height of 0.1 m is compared because these positions were the ones showing the highest and thereby most important velocities. The resulting speed for the experimental case and CFD prediction is shown in figure 6.3 on the facing page.

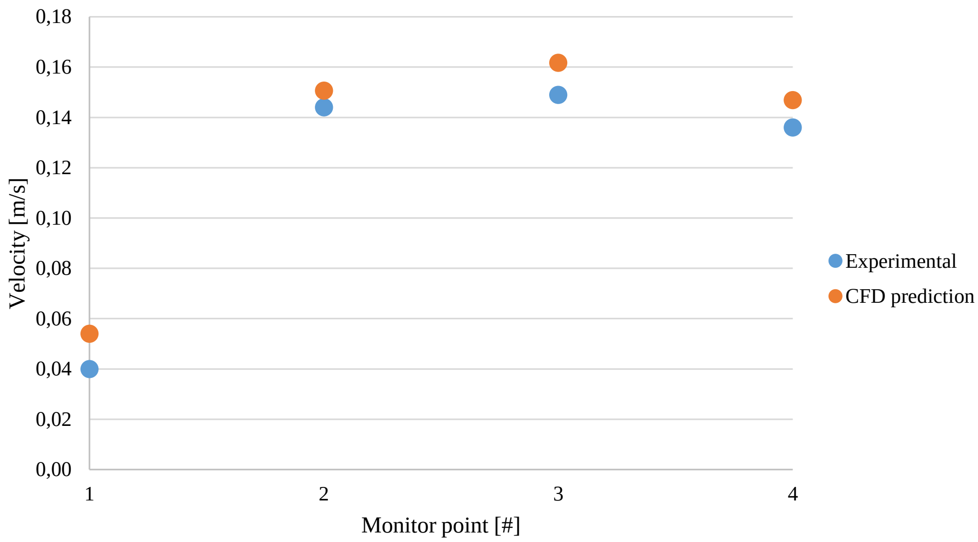

Figure 6.3. Velocities in experiment and reference model.

The results look fairly similar with the CFD prediction being slightly higher in all monitor points. For further validation, the vertical temperature gradient in the center of the room is compared, shown in figure 6.4. Even though values only in the points are known, curves are added for further understanding.

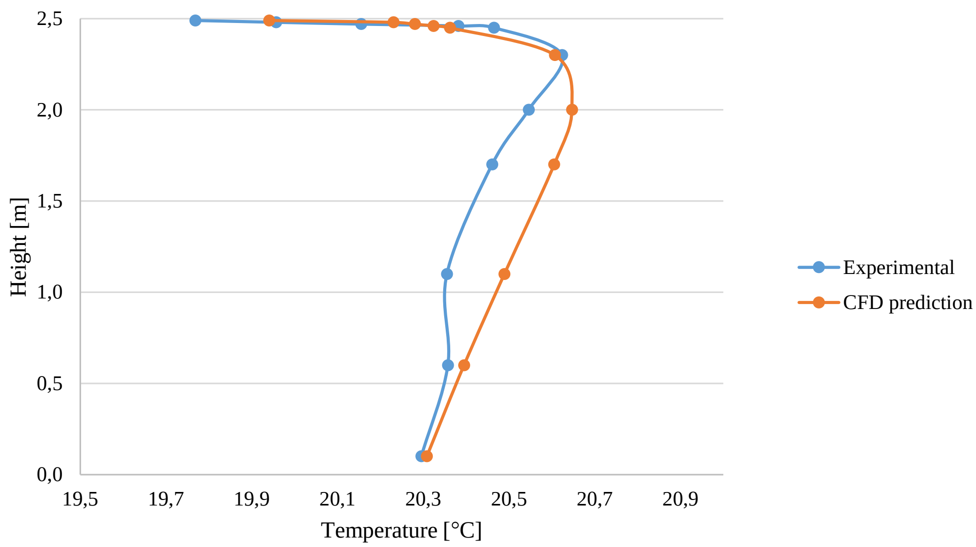

Figure 6.4. Vertical temperature gradient in the middle of the room in experiment and reference model.

Both figure 6.3 and 6.4 show good correlation between measurements and the reference CFD prediction. This validation form the foundation of the further CFD simulations in section 6.4 on the following page where some of the results from measurements are investigated further. First, the test conditions for the different simulations are presented.

6.3 Test conditions

In chapter 2 it was explained that the velocities in the room typically with diffuse ceiling ventilation, does not change when changing the flow rate. Experiments showed that maximum velocities increased slightly when changing the flow rate. This effect is tested by CFD and possible reasons why this phenomenon occurred are suggested. Furthermore the influence of room height is tested by comparing the reference model to a similar model, but with a room height of 4.4 m. Last, the difference in supply geometry is tested by comparing the high room with slot diffusers to a high room with diffuse ceiling (a large inlet occupying the entire ceiling area).

6.3.1 Test conditions

When changing the flow rate to the room, other boundary conditions also have to be changed, for instance the inlet temperature needs to be increased to compensate for the higher flow rate. Also, the surface temperatures of the walls, ceiling and floor change slightly. The boundary conditions for the four models, including reference model, are shown in table 6.6.

Case	q_0 [m^3/s]	ACH [h^{-1}]	t_s [°C]	t_{wall1} [°C]	t_{wall2} [°C]	t_{wall3} [°C]	t_{wall4} [°C]	t_{floor} [°C]	t_{ceiling} [°C]
1, 2.5 m, slots	0.055	2.84	16.33	21.02	19.98	20.24	20.31	20.67	19.62
2, 2.5 m, slots	0.179	9.23	17.34	20.50	19.59	19.76	19.81	19.99	19.08
3, 4.4 m, slots	0.055	1.61	16.33	21.02	19.98	20.24	20.31	20.67	19.62
4, 4.4 m, full	0.055	1.61	16.33	21.02	19.98	20.24	20.31	20.67	19.62

Table 6.6. Boundary conditions for the different CFD models.

6.4 Results

In chis section the results from the CFD simulations are presented and analysed. Main analysis is done on basis of visual presentations of the air flow and temperatures, but afterwards a short study of velocities and vertical temperature gradients in monitor points is performed.

The reference model is shown because this is the one comparisons are made to. There was a good correlation between reference model and obtained measurements.

6.4.1 Case 1 - low room with slot diffusers and flow rate of 0.055 m^3/s

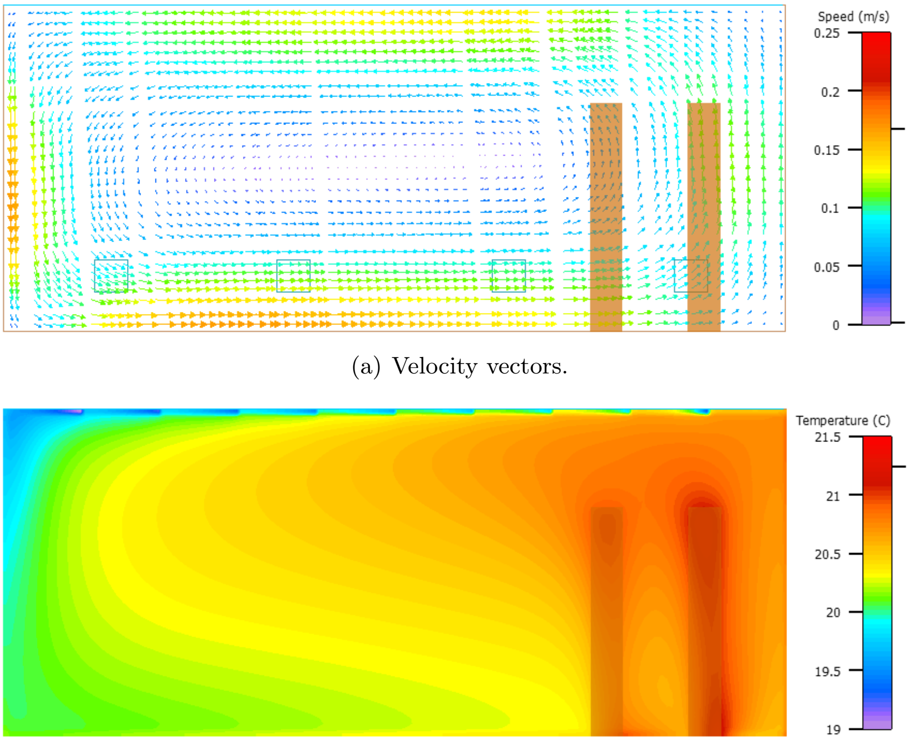

(a) Velocity vectors.

(b) Temperature scalar.

Figure 6.5. Reference model with slot diffusers and ACH of 2.8 h^{-1}.

Figure 6.5(a) shows that the velocities are high just below the ceiling, close to the wall opposite the heat loads and close to the floor. The temperature distribution also shows the direction of the flow, and that the flow mixes very quickly when entering the room. Maximum velocity measured in the occupied zone is 0.162 m/s. In figure 6.5(b) it is possible to see the flow direction and how the air mixes fast very close to the ceiling. Comparing the two figures, it is possible to see that the areas with high air velocity are also areas with cold air, relatively.

6.4.2 Case 2 - low room with slot diffusers and flow rate of 0.179 m^3/s

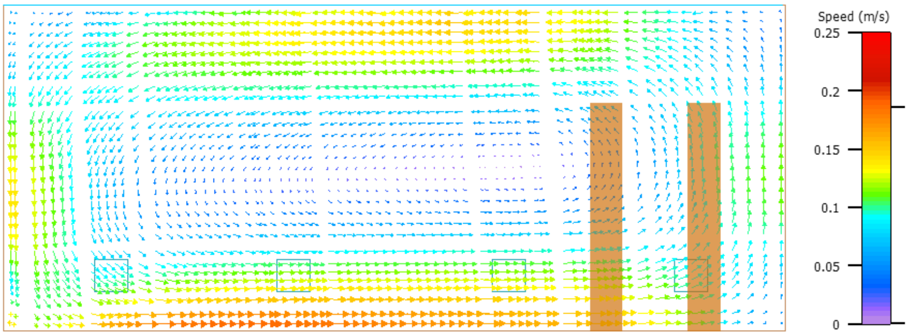

(a) Velocity vectors.

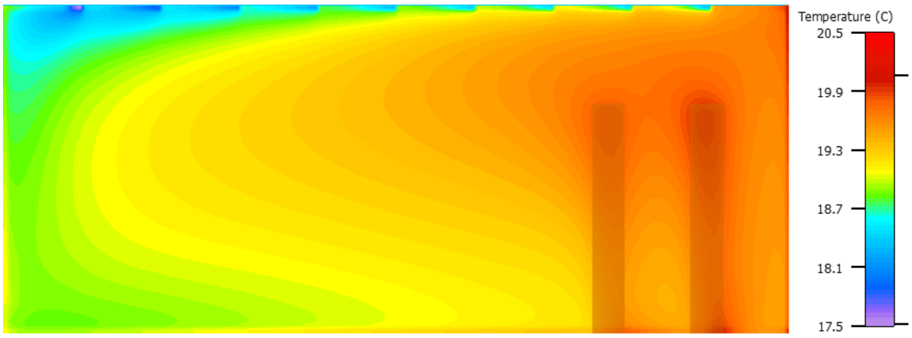

(b) Temperature scalar.

Figure 6.6. Low room model with slot diffusers and ACH of 9.2 h^{-1}.

Increasing the flow rate from 0.055 to 0.179 m^3/s increases the velocities in the room. So despite the inlet temperature being slightly higher than in the reference case, the velocities in the room are higher. Highest measured velocity in the occupied zone is 0.179 m/s. Velocities down the wall opposite the heat sources are lower than in the reference case, but velocities close to the floor higher. Looking at figure 6.6(b) the regions with cold air are smaller than in figure 6.5(b) on the previous page. This can indicate that it is an increase of momentum rather than cold air dropping towards the floor that creates an increase in velocities.

6.4.3 Case 3 - high room with slot diffusers and flow rate of 0.055 m^3/s

Having the same boundary conditions as in the reference case, the ceiling is raised to 4.4 m to see what difference that has in comparison to the reference model. Slot diffusers are still applied.

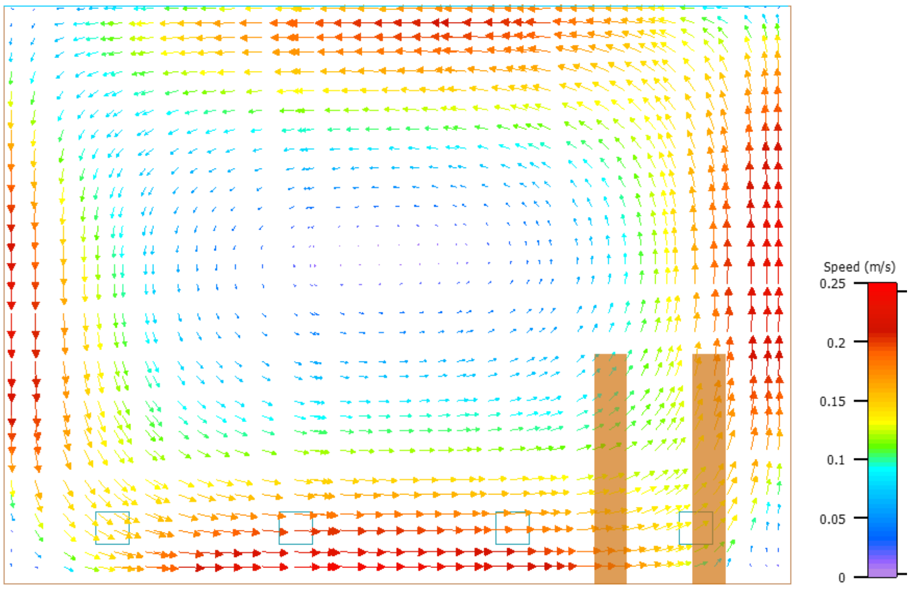

(a) Velocity vectors.

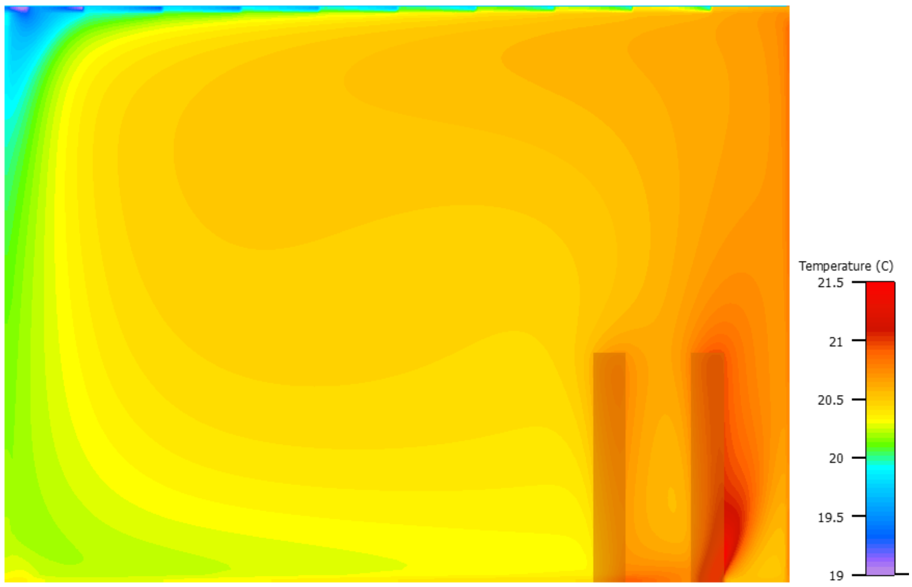

(b) Temperature scalar.

Figure 6.7. High room model with slot diffusers and ACH of 1.6 h^{-1}.

Velocities in general increase significantly, especially along the boundaries of the room. The results could indicate that the cold air flowing down close to wall 3 increases it's momentum from the ceiling towards the floor. Highest velocities in the occupied zone are 0.239 m/s.

6.4.4 Case 4 - high room with diffuse ceiling and flow rate of 0.055 m^3/s

During measurements the supply geometry was changed from a modular ceiling with small slots to a diffuse ceiling, where the air was supplied over the entire ceiling area. This is also tested in a CFD prediction shown in figure 6.8 on the following page.

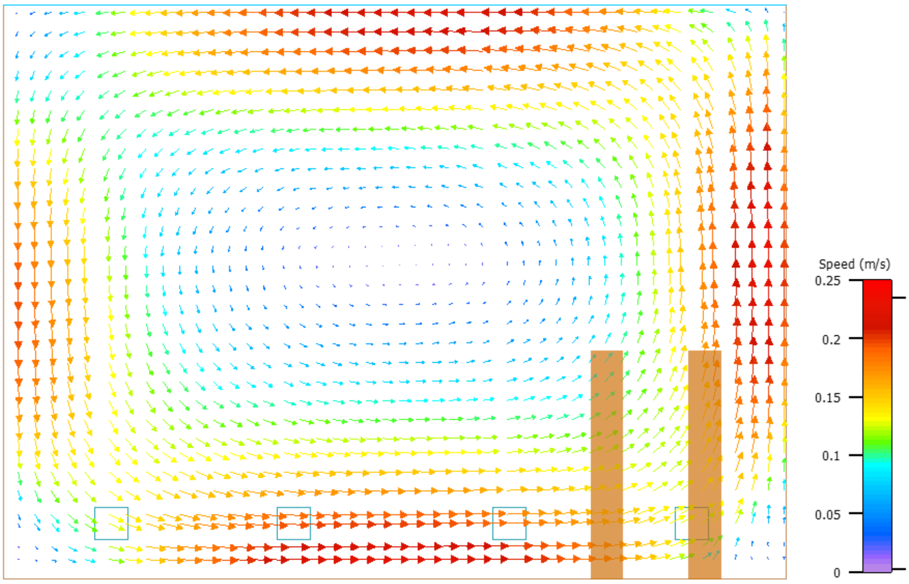

(a) Velocity vectors.

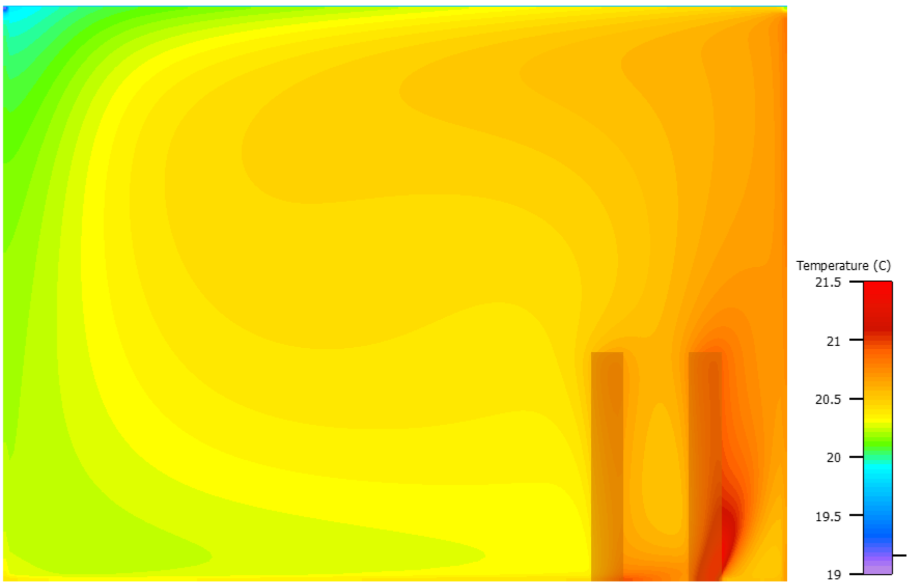

(b) Temperature scalar.

Figure 6.8. High room model with diffuse ceiling and ACH of 1.6 h^{-1}.

The tendencies are the same as in case 3, however it seems there is a better mixing close to the ceiling, meaning the air flowing downward of wall 3 have a lower density than in case 3 and therefore lower velocity. Case 4 has in general slightly lower velocities than case 3 with 0.224 m/s as the highest velocity in the occupied zone. The biggest differences are seen close to the ceiling. With the diffuse ceiling, the supply velocity is much lower, but the general flow pattern in the room does not indicate that the geometry of the supply opening is significant, as long as the velocities are as low as they are in these investigations.

These results correspond nicely to the ones measured in the experiment. With room heights of 4.1 m (slots) and 4.4 m (diffuse) the velocities measured were very similar. If the modular ceiling could have been tested in a height of 4.4 m instead of 4.1 m, the velocities would probably have been higher than the ones measured.

6.4.5 Comparison of models

The monitor points shown in figure 6.1 on page 61 are again used to compare the four models. A comparison of the velocities measured in the four points along the ground (monitor points 1, 2, 3 and 4) is shown in figure 6.9.

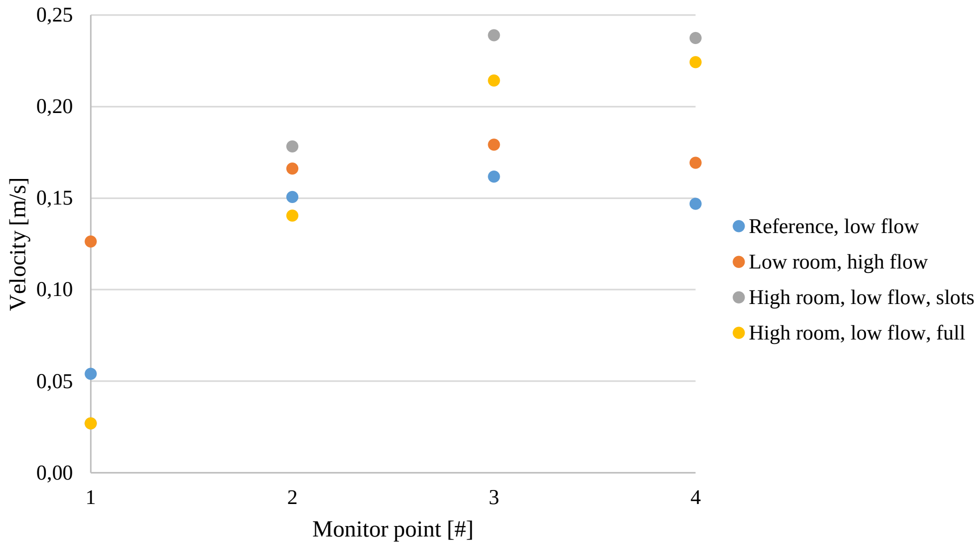

Figure 6.9. Comparison of velocities in four monitor points for the different models.

Also the vertical temperature gradients are compared, shown in figure 6.10.

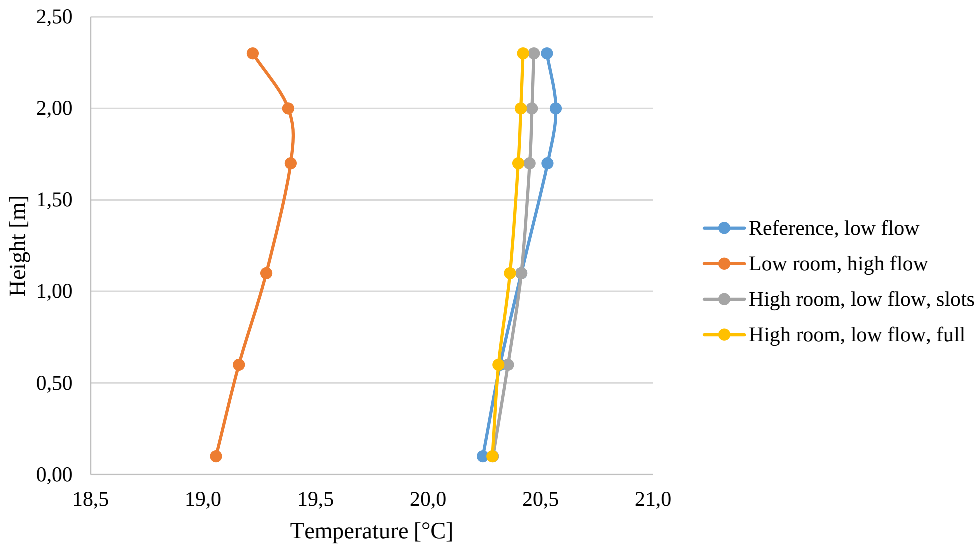

Figure 6.10. Comparison of vertical temperature gradients for the different models.

Figure 6.10 shows a very good mixing in the room in all cases, and a slightly better mixing with large room height than with lower room height.

Discussion 7

Many of the results were discussed in chapter 5, but some that were not and some that need a little extra attention are discussed in the following.

Generally the results show several a good connection to earlier studies performed by Nielsen [2007], Jakubowska [2009], Nielsen et al. [2010] and Chodor and Taradajko [2013]. Compared to measurements performed by Chodor and Taradajko [2013], resulting cooling capacities were slightly lower, however both showed that heat load distribution was vital for the conditions in the room. A reason why their cooling capacity was much higher can that they had a much higher heat load, in several cases above 2000 W. If some of these heat sources counteract each other, it seems to be possible to obtain low velocities even at very high heat loads. Nielsen [2007] compared several different types of air distribution systems, and when comparing the performances, a ceiling height of 2.5 m gave very similar results with heat loads either in the center of the room or evenly distributed. The comparison between the different heat load distributions showed just how much the heat sources dominate the flow pattern when utilising diffuse ceiling ventilation.

Nielsen [2007] claimed that when using diffuse ceiling ventilation, the flow pattern in the room would not be dependent on the flow rate, however results showed that especially with heat loads in one end of the room, an increase in flow rate gave an increase in air velocity. An explanation can be that when the air moves along the ceiling in a stable manner, the supply can add a small extra momentum, increasing the air velocity. The increase in air velocity happens even though the air is supplied with a higher temperature than with low flow rate, suggesting it is the momentum rather than buoyant flow from the drop caused by low temperatures. When creating design graphs, the mean product of q_0 and ΔT_0 was chosen. This naturally gives a higher performance than the situation measured with the highest air velocities. In a design situation, the situation giving the highest velocities should be selected.

A set of measurements were made to verify the use of the similarity principle to calculate the limits q_0 and ΔT_0 for the air distribution system, described in section 5.1 on page 35. The similarity principle prescribes that in case of fully developed turbulent flow, any non-dimensional velocity in the room is constant when keeping a constant $\Delta T_0/q_0$-ratio, which is also a constant Archimedes number. The results showed that despite keeping the $\Delta T_0/q_0$-ratio very close to constant, the dimensionless velocities were not completely constant from one experiment to another. Therefore, when creating the limiting curves in the design charts, one can not be entirely sure that this is the correct limit at a given heat load position.

It should still be emphasised that the change in air velocity at low and high flow rate is not very significant. As an example case 4a and 4d can be compared. The flow rate changed from 0.058 m^3/s to 0.292 m^3/s (by a factor 5) but air velocities in the occupied zone increased from 0.195 m/s to 0.254 m/s (by a factor 0.25). So it is fair to say the air velocities are slightly dependent on the flow rate. Having heat loads in other positions than in one end of the room showed much less influence on the air velocities when changing flow rate.

When performing measurements there are always some limitations which can give rise to some uncertainty. First of all precision of equipment is important, but also the way in which the experiments are conducted. Covering the entire occupied zone with measuring equipment would give a confidence that the entire air velocity pattern would be captures, but this is simply not possible. Finding the important positions of placing equipment is neither easy. In order to have more useful results, more measuring points in the occupied zone could have been investigated, so the equipment would be positioned evenly in the entire room as Chodor and Taradajko [2013] did.

One could ask why the three heat load distributions were selected. In other experiments, heat sources were positioned in order to simulate an office situation (Jakubowska [2009]) or people admiring a painting in a museum (Chodor and Taradajko [2013]). The reasons for choosing the different heat loads distributions are to have three entirely different heat load distributions which can be compared to each other by means of the cooling capacity of the air distribution system. What they simulate is up to each individual to decide but they give a clear idea about what happens in certain situations.

Conclusion 8

In the conclusion the results obtained through experimental and numerical analysis are summed up, and a few future perspectives are presented.

In the review of previous studies, diffuse ceiling ventilation was highlighted as a type of air distribution system with an ability to remove large thermal loads without compromising the indoor climate. A study conducted by Chodor and Taradajko [2013] showed signs of issues occur when operating in a room with large height. They also showed that dependent on the heat load distribution, the system would perform differently.

In order to evaluate the performance of the air distribution system, the conditions in the room was evaluated based on the maximum air velocity in the occupied zone. By use of the similarity principle the flow rate q_0 and temperature difference between supply and return ΔT_0 was recalculated to fit the selected limit for maximum air velocity of 0.15 m/s. Before conducting experiments to evaluate the different set-ups, it was tested whether or not the similarity principle could be used to recalculate q_0 and ΔT_0. Results showed that non-dimensional velocities changes slightly despite keeping a constant ratio of $\Delta T_0/q_0^2$, a constant Archimedes number. Deviations were so small that the similarity principle was still used, however for each experimental case several different test conditions q_0,ΔT_0 were investigated.

In this study experiments were made in order to investigate the importance of three parameters in a room air distribution system, namely room height, heat load distribution and supply geometry. Experiments were carried out in a test room with three different room heights, three different heat load distributions and different supply geometry. An acoustic ceiling in a height of 4.4 m was compared to a modular ceiling of stone wool elements in heights of 2.5 m and 4.1 m.

By comparing results for ceiling heights of 4.1 m (modular ceiling) and 4.4 m (diffuse acoustic ceiling) the differences in performance were insignificant, however when comparing these results those of a room height of 2.5 m (modular ceiling), there was a large difference. With a lower room height the cooling capacity was much higher.
Comparing the three heat load distributions to each other, significant differences were also observed. With heat sources in the middle of the room and evenly distributed showed quite similar results, while having heat loads in one end significantly increased the air velocities. Also, an increase in air velocities was observed when increasing the flow rate, indicating the flow in the room was slightly dependent on the flow rate and not only the strength of the heat sources.
Other than smoke experiments, the air velocity and temperature distribution measured in the room confirmed theories about the flow pattern in given situations, however with evenly distributed heat sources (and slightly with heat sources in the middle of the room), measured velocities were unstable, or one could say they were periodically stable.
The worst conditions in any test was measured with a high flow rate, diffuse acoustic

ceiling, room height of 4.4 m and heat loads in one end of the room. Only this single test gave a draught rating of >20%.

CFD simulations were made to back-up the results measured in the experimental part. After verifying the CFD reference model with experimental results, four simulations were set up, and results compared to the reference model. Simulations showed very good correlation with measurements, and indicate that room height have a large influence on velocities in the room, but also that changing supply geometry have a small effect, at least with such low-velocity supplies as the ones tested.

Generally, the results showed that with a low room height, the system performed similarly to earlier studies. Main conclusion is that both room height and heat load distribution have a great influence on the thermal indoor climate when using diffuse ceiling ventilation as air distribution system.

Bibliography

BR, 2010. BR. *The Danish Ministry of Economic and Business Affairs - Danish Building Regulations*, URL: `http://bygningsreglementet.dk`, 2010. Downloaded: 06-06-2014.

Chodor and Taradajko, 2013. Anna Diana Chodor and Piotr Paweł Taradajko. *Experimental and Numerical Analysis of Diffuse Ceiling Ventilation*, 2013. Master's Thesis, Aalborg University.

DS/CEN/CR 1752, 2001. DS/CEN/CR 1752. *Ventilation for buildings - Design criteria for the indoor environment*, 2001.

DS/EN 13779, 2007. DS/EN 13779. *Ventilation for non-residential buildings - Performance requirements for ventilation and room-conditioning systems*, 2007.

DS/EN 15251, 2007. DS/EN 15251. *DS/EN 15251 - Indoor environmental input parameters for design and assessment of energy performance of buildings addressing indoor air quality, thermal environment, lighting and acoustics*, 2007.

DS/EN ISO 7726, 2001. DS/EN ISO 7726. *Ergonomics of the thermal environment - Instruments for measuring physical quantities*, 2001.

DS/EN ISO 7730, 2006. DS/EN ISO 7730. *Ergonomics of the thermal environment - Analytical determination and interpretation of thermal comfort using calculation of the PMV and PPD indicies and local thermal comfort criteria*, 2006.

Hyldgård, Funch, and Steen-Thøde, 1997. Carl Erik Hyldgård, E.J. Funch, and M. Steen-Thøde. *Grundlæggende Klimateknik og Bygningsfysik*. ISSN: 1395-8232 U9714. Aalborg University, 1997.

Jacobs, Oeffelen, and Knoll, 2008. Piet Jacobs, Elisabeth C.M. van Oeffelen, and Bas Knoll. *Diffuse ceiling ventilation, a new concept for healthy and productive classrooms*, 2008. Indoor Air 2008, Copenhagen, Denmark, 2008.

Jakubowska, 2009. Ewa Jakubowska. *Air distribution in Rooms with Diffuse Ceiling Inlet*, 2009.

Mentor Graphics, 2012. Mentor Graphics. *FloVENT User guide - Software Version 9.3*, 2012.

Müller, Kandzia, Kosonen, Melikov, and Nielsen, 2013. Dirk Müller, Claudia Kandzia, Risto Kosonen, Arsen Krikor Melikov, and Peter Vilhelm Nielsen. *Mixing ventilation: Guide on mixing air distribution design*, 2013.

Nielsen, Allard, Awbi, Davidson, and Schälin, 2007. Peter V. Nielsen, Francis Allard, Hazim B. Awbi, Lars Davidson, and Alois Schälin. *Computational Fluid Dynamics in Ventilation Design*. ISBN: 2-9600468-9-7. Rehva, 2007.

Nielsen, 2011. Peter Vilhelm Nielsen. *The "Family Tree" of Air Distribution Systems*, 2011.

Nielsen, 1999. Peter Vilhelm Nielsen. *Lecture Notes on Scale-Model Experiments.* ISSN: 1395-8232 U9913. Department of Building Technology and Structural Engineering, Aalborg University, 1999.

Nielsen, 2007. Peter Vilhelm Nielsen. *Analysis and Design of Room Air Distribution Systems*, 2007.

Nielsen, Jensen, and Rong, 2010. Peter Vilhelm Nielsen, Rasmus Lund Jensen, and Li Rong. *Diffuse Ceiling Inlet Systems and the Room Air Distribution*, 2010. Clima 2010, 10th REHVA World Congress, 9.-12. May, Antalya.

The Engineering Toolbox, 2014. The Engineering Toolbox. *Manning's Roughness Coefficient.* URL: `kortlink.dk/engineeringtoolbox/edrh`, 2014. Downloaded: 28-05-2014.

Yang, 2011. Honglu Yang. *Experimental and Numerical Analysis of Diffuse Ceiling Ventilation*, 2011. Master's Thesis, Technical University of Denmark.